

This manuscript has been published in *Biointerphases*, 2015 Sep 15;10(3):031002. doi:
10.1116/1.4926442.

Title: Self-etching Zinc-doped adhesives improve the potential of caries-affected dentin to be functionally remineralized.

Short title: Bioactivity of Zn-doped self-etching adhesives in caries-affected dentin.

Authors: Manuel Toledano^{1*}, Fátima S. Aguilera¹, Estrella Osorio¹, Inmaculada Cabello¹, Manuel Toledano-Osorio¹, Raquel Osorio¹.

Institution: ¹University of Granada, Faculty of Dentistry, Dental Materials Section.

Address: ¹University of Granada, Faculty of Dentistry, Dental Materials Section
Colegio Máximo de Cartuja s/n
18071 – Granada - Spain.

*Corresponding author: Prof. Manuel Toledano

University of Granada, Faculty of Dentistry

Dental Materials Section

Colegio Máximo de Cartuja s/n

18071 – Granada - Spain.

Tel.: +34-958243788

Fax: +34-958240809

Email: toledano@ugr.es

ABSTRACT

The aim of this study was to evaluate if mechanical cycling influences bioactivity at the resin-carious dentin interface after bonding with Zn-doped self-etching adhesives. Caries-affected dentin (CAD) surfaces were bonded with: Clearfil SE Bond (SEB), and 10 wt% ZnO nanoparticles or 2 wt% ZnCl₂ were added into the SEB primer or bonding components. Bonded interfaces were stored during 24 h, and then tested or submitted to mechanical loading. Microtensile bond strength (MTBS) was assessed. Debonded dentin surfaces were studied by field emission scanning electron microscopy (FESEM). Remineralization of the bonded interfaces was evaluated through nanohardness (Hi) and Young's modulus (Ei), Raman spectroscopy/cluster analysis, and Masson's trichrome staining technique. Load cycling increased the percentage of adhesive failures. New precipitation of minerals composed of zinc-base salts and multiple Zn-rich phosphate deposits were observed in samples infiltrated with the Zn-doped adhesives. At the hybrid layer, specimens treated with ZnO incorporated in the primer (SEB·P-ZnO), after load cycling, attained the highest Ei and Hi. Load cycling increased Ei at the bottom of the hybrid layer when both, SEB un-doped and SEB with ZnCl₂ included in the bonding (SEB·Bd-ZnCl₂), were used. ZnO incorporated in the primer promoted an increase in height of the phosphate and carbonate peaks, crystallinity, relative mineral concentration, and lower collagen crosslinking. ZnCl₂ included in the bonding attained similar results, but relative mineral concentration decreased, associated to higher crosslinking and restricted collagen maturation. Staining techniques permitted to observe no signs of exposed protein at the resin-dentin interface after using SEB·P-ZnO.

Key words: Self-etching adhesives, load cycling, zinc, remineralization, dentin.

I. INTRODUCTION

The formation of dentin caries is an intricate process associated with dynamic events of mineral loss and gradual denaturation of collagen fibrils¹. The infected layer^{2,3}, which was found to be comprised of denatured collagen that has lost the potential for remineralization, becomes the consensus target for removal. Conversely, the affected layer, which is partially demineralized and remineralizable with collagen fibrils retaining their natural structure around intact dentinal tubules, is to be preserved to maximize reparative potential and to reduce the risk of pulp exposure^{4,5}.

Therapeutic dentin demineralization or conditioning *vs* etching, and further resin infiltration are clinically required to promote resin-dentin bonding, aimed to repair the decayed dental substrate. The concept of self-etching adhesives (SEAs) is based on the use of polymerizable acidic monomers that simultaneously condition and prime dentin. After dentin demineralization, mineral ions are removed from the apatite latticework (*i.e.* inorganic matrix), resulting in exposure of the collagen matrix (mainly type I collagen fibrils)⁶. The bonding mechanism of SEAs is based on micro-mechanical interlocking along with a chemical interaction of functional monomers with calcium⁷. Functional monomers represent the main active components of SEAs, facilitating the simultaneous etching and priming of the hard tooth substrate with inward diffusion of co-monomers^{7,8}. Some portions of collagen fibers are solubilized or hybridized, as a part of the hybrid complex⁹. Commonly, functional monomers in SEAs are acidic esters, originating from the reaction of a bivalent alcohol with methacrylic acid and phosphoric/carboxylic acid derivatives¹⁰. Yoshihara et al. (2011)^{11,12} showed that SEAs containing the phosphoric-acid ester functional monomer 10-MDP (10-methacryloyloxi-decyl-dihydrogen-phosphate) create a nano-layered structure at the adhesive-dentin interface, having been associated with outstanding bond integrity and

clinical longevity¹³. Additionally, the use of methacrylate phosphate monomer on type-I collagen has been intended to mimic the role of phosphoproteins that act as the template for the nucleation and growth of apatite in natural dentin¹⁴.

Adhesive-dentin interfaces may be degraded by absorbed water from the host dentin *via* tubules or through nano-leakage¹⁵. 10-MDP appeared hydrolytically unstable in water; it can degrade to hydroxydecyl dihydrogen phosphate and methacrylate¹⁰. Since SEAs contain water, such monomer hydrolysis, and the ensuing additional collagen exposure, is expected to compromise their clinical performance¹⁶. When collagen is exposed, endogenous matrix metalloproteinases (MMPs) contribute to degradation of collagen fibrils, in particular within incompletely resin-infiltrated hybrid layers¹⁷. Spectroscopic results confirm that majority of demineralized dentin matrix in both sound and CAD was not protected by the adhesive¹⁸. Ryou et al. (2011)¹⁹, have recently demonstrated that the remineralization of such demineralized zones within the hybrid layers may be a potential means for preserving the durability of the resin-dentin interface^{19,20}.

The use of zinc-containing materials may reduce the collagen degradation mediated by MMPs within the poorly infiltrated hybrid layers and carious dentin by protecting sensitive cleavage sites of collagen within the demineralized dentin²¹. Zinc may not only act as an inhibitor of MMPs, but may also influence signaling pathways and stimulate a metabolic effect in hard tissue mineralization²². It may also be that effective inhibitors of MMPs included in resin-dentin bonding interfaces may protect the seed crystallite-sparse collagen from degradation, allowing them to become remineralized²³. Zinc has also been shown to inhibit dentin demineralization²⁴. These effects make zinc attractive for use as therapeutic agent in the fields of hard and soft tissue engineering. Thereby, the contemporary idea of minimally invasive operative treatment, where

therapeutic restorations are performed to combat the carious process and remineralize the dental hard tissues, may be satisfied by using such resin-base and Zn-doped systems.

Nano-indentation has recently been used for the examination of tooth structure, measuring both hardness and elastic modulus ²⁵. Dentin mineral is composed by carbonate-substituted calcium hydroxyapatite crystals and magnesium organized in a crystal lattice; this lattice structure affords the mechanical properties of the healthy and carious tissue. The vast majority of the work has been focused on the histological, microscopic and mechanical aspects of carious dentin, but rarely on the underlying molecular structure which is integral to a full understanding of the disease, especially its effect on the mineral content and collagen matrix ²⁶. In this respect, Raman is a powerful tool in generating direct information about the molecules of a sample. Compared to the conventional histological and microscopic methods Raman spectroscopy and cluster analysis result advantageous because they are fast, non-intrusive, stain-free, quantitative and less prone to human subjectivity.

The innovative Zn-doped light-curable materials to be tested in this study might be able to induce a therapeutic remineralizing effect on the partially demineralized resin-dentin interface. This investigation assessed the bond strength, chemical interaction and mechanical performance of caries-affected dentin surfaces treated with Zn-doped SEAs. “The two null hypotheses to be tested were that bond strength and remineralization of the resin-dentin interface of the tested SEAs would not be influenced by: (1) incorporation of zinc into the chemical formulations of the adhesive or (2) application of mechanical load cycling on restored teeth.”

II. MATERIAL AND METHODS.

A. Specimen preparation, bonding procedures and mechanical loading

Ninety human third molars with occlusal caries were obtained with informed consent from donors (20–40 year of age), under a protocol approved by the Institution Review Board. Molars were stored at 4°C in 0.5% chloramine T for up to 1 month before use. A flat mid-coronal carious dentin surface was exposed using a hard tissue microtome (Accutom-50; Struers, Copenhagen, Denmark) equipped with a slow-speed, water-cooled diamond wafering saw (330-CA RS-70300, Struers, Copenhagen, Denmark). The inclusion criteria for carious teeth were that the caries lesion, surrounded by sound dentin, should be limited to the occlusal surface, that it extended at least half the distance from the enamel-dentin junction to the pulp chamber. To obtain caries-affected dentin, grinding was performed by using the combined criteria of visual examination, surface hardness using a dental explorer, and staining by a caries detector solution (CDS, Kuraray Co., Ltd., Osaka, Japan). Using this procedure it was removed all soft, stainable, carious dentin. It was left the relatively hard, caries-affected non staining dentin, on the experimental side. A 180-grit silicon carbide (SiC) abrasive paper mounted on a water-cooled polishing machine (LaboPol-4, Struers, Copenhagen, Denmark) was used to produce a clinically relevant smear layer²⁷. A two-step self-etching system, Clearfil SE Bond (Kuraray, Tokyo, Japan) (SEB) was tested. It was zinc doped by mixing the primer of SEB (SEB·P) with 10 wt% ZnO microparticles (1 to 2 microns) (Panreac Química, Barcelona, Spain) were added to the primer of SEB (SEB·P) (SEB·P-ZnO) or to the bonding resin (SEB·Bd) (SEB·Bd-ZnO); or 2 wt% of ZnCl₂ crystals (Sigma Aldrich, St. Louis, MO, USA) were actively dissolved into the primer (SEB·P) (SEB·P-ZnCl₂) or into the bonding resin (SEB·Bd) (SEB·Bd-ZnCl₂). To achieve complete dissolution of ZnCl₂ and dispersion of ZnO particles, adhesive blends were vigorously shaken 1 min in a tube agitator (Vortex Wizard 51075; Velp Scientifica, Milan, Italy). The complete process was performed in the dark. Preparation

of the adhesives and zinc concentrations were based upon previous studies^{17,28,29}. The chemical and descriptions of the adhesives are provided in Table I.

Table I. Materials and chemicals used in this study and respective manufacturers, basic formulation and mode of application.

Product details	Basic formulation	Mode of application
Clearfil SE Primer and Bond (SEB) (Kuraray, Japan)	Primer (SEB•P) MDP, HEMA, camphorquinone, N, N-Diethanol-p-toluidine, water Bond (SEB•Bd) Bis-GMA, MDP, HEMA, camphorquinone, N, N-Diethanol-p-toluidine, Silanated colloidal silica	Adhesive application Rinse with water Air-dry (5 s) Primer application (20 s) Air-dry (3 s) Bond application (10s) Light activation (15 s)
Zinc oxide (ZnO) (Panreac Química SA, Barcelona, Spain).		
Zinc chloride 2-hydrate powder (ZnCl ₂) (Sigma Aldrich, St. Louis, MO, USA).		
X-Flow™ (Dentsply, Caulk, UK)	Strontium alumino sodium fluorophosphorsilicate glass, di- and multifunctional acrylate and methacrylate resins, DGDMA, highly dispersed silicon dioxide UV stabilizer, ethyl-4-dimethylaminobenzoate camphorquinone, BHT, iron pigments, titanium dioxide	
SBFS (pH=7.45)	NaCl 8.035 g (Sigma Aldrich, St. Louis, MO, USA). NaHCO ₃ 0.355 g (Sigma Aldrich, St. Louis, MO, USA). KCl 0.225 g (Panreac Química SA, Barcelona, Spain). K ₂ HPO ₄ ·3H ₂ O 0.231 g, MgCl ₂ ·6H ₂ O 0.311 g (Sigma Aldrich, St. Louis, MO, USA) 1.0 M – HCl 39 ml (Sigma Aldrich, St. Louis, MO, USA) CaCl ₂ 0.292 g (Panreac Química SA, Barcelona, Spain). Na ₂ SO ₄ 0.072 g (Panreac Química SA, Barcelona, Spain). Tris 6.118 g (Sigma Aldrich, St. Louis, MO, USA) 1.0 M – HCl 0–5 ml (Panreac Química SA, Barcelona, Spain).	

Abbreviations: MDP: Methacryloyldodecylphosphate; HEMA: 2-hydroxyethyl methacrylate; Bis-GMA: bisphenol A diglycidyl methacrylate; DGDMA: diethyleneglycol dimethacrylate phosphate; BHT: butylated hydroxytoluene; SBFS: simulated body fluid

solution; NaCl: sodium chloride; NaHCO₃: sodium bicarbonate; KCl: potassium chloride; K₂HPO₄·3H₂O: potassium phosphate dibasic trihydrate; MgCl₂·6H₂O: magnesium chloride hexahydrate; HCl: hydrogen chloride; CaCl₂: Calcium chloride; Na₂SO₄: sodium sulfate; Tris: tris(hydroxymethyl) aminomethane; SBFS: simulated body fluid solution; NaCl: sodium chloride; NaHCO₃: sodium bicarbonate; KCl: potassium chloride; K₂HPO₄·3H₂O: potassium phosphate dibasic trihydrate; MgCl₂·6H₂O: magnesium chloride hexahydrate; HCl: hydrogen chloride; CaCl₂: Calcium chloride; Na₂SO₄: sodium sulfate; Tris: tris(hydroxymethyl) aminomethane.

The specimens were divided into the following main groups (n=8) based on the tested adhesive systems: (i) Group SEB: Clearfil SEB; (ii) Group SEB·P-ZnO: SEB·P-ZnO was applied followed by the resin bonding (SEB·Bd); (iii) Group SEB·P-ZnCl₂: SEB·P-ZnCl₂ was applied followed by de resin bonding (SEB·Bd); (iv) Group SEB·Bd-ZnO: SEB·Bd-ZnO was applied after the primer (SEB·P) placement, and (v) Group CSEB·Bd-ZnCl₂: CSEB·Bd-ZnCl₂ was applied after the primer (SEB·P) placement. The bonding procedures were performed in moist caries-affected dentin following the manufacturer's instructions. A flowable resin composite (X-Flow™, Dentsply, Caulk, UK) was placed incrementally in five 1 mm layers and light-cured with a Translux EC halogen unit (Kulzer GmbH, Bereich Dental, Wehrheim, Germany) for 40 s. Half of the carious teeth were stored for 24 h in simulated body fluid (SBF) (ISO 23317 method), and the other half were submitted to mechanical loading, in SBF (100,000 cycles, 3 Hz, 49 N) (S-MMT-250NB; Shimadzu, Tokyo, Japan)³⁰. The cycling compressive load was perpendicularly applied to the flat resin composite build-ups using a 5-mm diameter spherical stainless steel plunger, while immersed in deionized water³¹. The load cycling lasted for 9 hours and 15 minutes; the rest of the time until complete 24 h, the loaded specimens were kept in SBF, at 37 °C.

B. Microtensile Bond Strength

After the different procedures, 40 teeth (four from each group) were sectioned into serial slabs, perpendicular to the bonded interface to produce bonded sections of, approximately, 1.0 mm thick. This yielded about three slabs of bonded caries-affected dentin *per* tooth. Twelve slabs from each experimental group were used for bond

strength evaluation. Slabs were hand trimmed with a fine diamond bur into hourglass-shaped specimens, with the smallest dimension at the bonded interface (1mm²). This trimming technique was chosen in order to accurately delimit the bonded tissue of interest (caries-affected dentin). Specimens were attached to a modified Bencor Multi-T testing apparatus (Danville Engineering Co., Danville, CA) with a cyanoacrylate adhesive (Zapit/Dental Venture of America Inc., Corona, CA, USA) and stressed to failure in tension (Instron 4411 /Instron Inc., Canton, MA, USA) at a crosshead speed of 0.5 mm/min. The cross-sectional area at the site of failure of the fractured specimens was measured to the nearest 0.01mm with a pair of digital calipers (Sylvac Ultra-Call III, Fowler Co Inc., Newton, Mass, USA). Bond strength values were calculated in MPa.

Fractured specimens were examined with a stereomicroscope (Olympus SZ-CTV, Olympus, Tokyo, Japan) at 40x magnification to determine the mode of failure. Failure modes were classified as adhesive or mixed. Representative specimens of each group were fixed in a solution of 2.5% glutaraldehyde in 0.1 mol/L sodium cacodylate buffer for 24 h, rinsed three times in 0.1 mol/L sodium cacodylate buffer. Samples were placed in an apparatus for critical point drying (Leica EM CPD 300, Wien, Austria). They were then sputter-coated with carbon by means of a sputter-coating Nanotech Polaron-SEMPREP2 (Polaron Equipment Ltd., Watford, UK) and observed with a field emission scanning electron microscope (FESEM Gemini, Carl Zeiss, Oberkochen, Germany) at an accelerating voltage of 3 kV. Energy-dispersive analysis was performed in selected points using an X-ray detector system (EDX Inca 300, Oxford Instruments, Oxford, UK) attached to the FESEM. MTBS values were analyzed by two-way ANOVA (independent factors were mechanical loading and adhesive type) and

Student Newman Keuls multiple comparisons tests. For all tests, statistical significance was set at $\alpha = 0.05$.

C. Measurement of nanohardness and Young's modulus

Thirty molars were used for the test. An atomic force microscope (AFM- Nanoscope V, Digital Instruments, Veeco Metrology group, Santa Barbara, CA, USA) equipped with a Triboscope indenter system (Hysitron Inc., Minneapolis, MN, USA) and a Berkovich indenter (tip radius 20 nm) was employed for the indentation process in a fully hydrated status³². For each subgroup, three slabs were tested. On each slab, five indentation lines were executed in two different occluso-gingival positions exactly located at the HL and the BHL, in a straight line. Indentations were performed with a load of 4000 nN and a time function of 10 s³³. Hardness (Hi) and modulus of elasticity (Ei) data were registered in GPa. Data were analyzed by two-way ANOVA (independent factors were mechanical loading and adhesive procedure) and Student–Newman–Keuls multiple comparisons ($P < 0.05$).

D. Raman spectroscopy and cluster analysis

A dispersive Raman spectrometer/microscope (Horiba Scientific Xplora, Villeneuve d'Ascq, France) was also used to analyze bonded interfaces. A 785-nm diode laser through a X100/0.90 NA air objective was employed. Raman signal was acquired using a 600-lines/mm grating centered between 900 and 1,800 cm^{-1} . Chemical mapping of the interfaces were performed. For each specimen a 25 μm x 25 μm area of the interfaces at different sites were mapped using 1.8 μm spacing at X axis and 1 μm at Y axis. Chemical mapping was submitted to K-means cluster (KMC) analysis using the multivariate analysis tool (ISys® Horiba), which includes statistical pattern to derive the independent clusters. Hypotheses concerning the number of clusters formed in resin-

bonded interfaces were previously obtained ³⁴. However, Ward's method was employed to get some sense of the number of clusters and the way they merge from the dendrogram. The aim of a factor analysis lies in the effective reduction of the dataset dimension while maintaining a maximum of information. This method was used to model the data and to determine spectral variances associated for data differentiation. The K-means clustering is a method of analysis based on a centroid model which aims to partition n observations into k clusters in which each observation belongs to the cluster with the nearest mean ³⁵. The natural groups of components (or *data*) based on some similarity and the centroids of a group of *data* sets were found by the clustering algorithm once calculated by the software. To determine cluster membership, this algorithm evaluated the distance between a point and the cluster centroids. The output from a clustering algorithm was basically a statistical description of the cluster centroids with the number of components in each cluster. The biochemical content of each cluster was analyzed using the average cluster spectra. Four clusters were identified and values for each cluster such as adhesive (ADH), hybrid complex (HY COM) and dentin (DEN1, DEN2), within the interface, were independently obtained. Principal component analysis (PCA) decomposed *data* set into a bilinear model of linear independent variables, the so-called principal components (PC_S). The observed spectra were performed with 10 complete overlapping Gaussian lines, suggesting homogeneous data for further calculations ^{36,37}. As the cluster centroids are essentially means of the cluster score for the elements of cluster, the mineral and organic components of dentin hybrid layers were examined for each cluster. A comparison of the spectra that were collected from the two specimens which compose each subgroup indicated complete overlap, suggesting similarity between both measurements. At this point, the mineral and organic

component of dentin, and the degree of the adhesive presence, at the resin-CAD interface was analyzed as follows:

Relative presence of mineral:

1. *Phosphate (960 cm⁻¹) and carbonate (1070 cm⁻¹) peaks and areas of their bands.*

Peak heights were processed in absorbance units.

2. *Relative mineral concentration (RMC) (i.e., mineral-to-matrix ratio):* It was inferred from the visible ratio of the intensities of the peaks at 960 cm⁻¹ (phosphate) (PO₄³⁻) and 1003 cm⁻¹ (phenyl group), the aromatic ring of phenylalanine residues in collagen. These indexes concerned with the maximum relative degree of mineralization^{38,39}.

Crystallinity: It was evaluated based on the full width at half maximum (FWHM) of the phosphate band at 960 cm⁻¹. This index expressed the crystallographic or relative atomic order, since narrower peaks suggest less structural variation in bond distances and angles³⁸. In general, the narrower the spectral peak width is, the higher the degree of mineral crystallinity³⁹.

Gradient in mineral content (GMC), or carbonate content of the mineral crystallites: It was assessed as the relationship between the ratio of heights at 1070 cm⁻¹ (carbonate) (CO₃²⁻) to 960 cm⁻¹ (phosphate) (PO₄³⁻), indicating carbonate substitution for phosphate³⁸.

Modified phosphate peaks ratio (mPPR): it assesses the ratio between the mineral peak at 960 cm⁻¹ (phosphate) (PO₄³⁻), within the demineralized zone and the mineral peak (PO₄³⁻) within the caries-affected dentin substratum⁴⁰.

The organic component of dentin was analyzed examining the following parameters:

Normalization: Phenyl group: The peak at 1003 cm⁻¹, which is assigned to C-C bond in the phenyl group, was used for normalization⁶.

Crosslinking:

1. Pyridinium ring vibration: In the spectra, the peak appeared at 1030/1032.7 cm^{-1} , is assigned to the C-C in pyridinium ring vibration which has a trivalent amino acid crosslinking residue ⁴¹. The relative intensity of this peak increases after the crosslinking formation ⁴².
2. Ratio Pyridinium/Phenyl (1032 cm^{-1} /1001 cm^{-1}): the higher the ratio, the greater the extend of collagen cross-linking ^{42,43}.
3. Ratio 1003 (phenyl)/1450 (CH_2): arises preceding deposition of HAP (hydroxyapatite) crystals within the structure ⁴⁴.
4. AGEs (advance glycation end products)-pentosidine at 1550 cm^{-1} , interpreted as a marker of the aging process ⁴⁵.

Nature of collagen:

1. Amide III, CH_2 and amide I: The peaks at 1246/1270, 1450 and 1655/1667 cm^{-1} , assigned to amide III, CH_2 and amide I, respectively, are sensitive to the molecular conformation of the polypeptide chains ^{6,42,43}. The decrease of amide I peak indicates damage or removal of collagen fibrils ⁴³.
2. Ratio amide I/amide III concerned the organization of collagen.
3. Ratio amide III / CH_2 wagging mode indicates the structural differences ⁴⁶.
4. Ratio amide I/ CH_2 indicates altered collagen quality ⁴⁶.
5. Ratios amide III and I/AGEs-Pentosidine, indicatives of the glycation reaction vs collagen scaffolding ⁴⁶.
6. 1340 cm^{-1} peak: This signal has been assigned to protein α -helices where intensity is sensitive to molecular orientation ⁴⁴.

Degree of adhesive presence:

1. *Degree of conversion of adhesive*: Ratio 1637/1608. The peak appearing at 1637 cm^{-1} is associated with C=C of methacrylate, and the peak at 1608 cm^{-1} is related to C-C in phenyl of adhesive monomer⁴³.
2. *Bis-GMA penetration*: Ratio 1113/1667. The peak appearing at 1113 cm^{-1} is associated with C-O-C of adhesive, and the peak at 1667 cm^{-1} is related to amide I^{43,47}.
3. *Adhesive (Bis-GMA and HEMA) penetration*: Ratio 1454/1667. The peak appearing at 1454 cm^{-1} is assigned to the CH₂ group of both Bis-GMA and HEMA, and the peak at 1667 cm^{-1} is related to amide I^{43,47}.
4. *Others*: The peak at 1720 cm^{-1} is associated at carbonyl group. The peak at 1453 cm^{-1} is associated at CH₂ def^{43,47}.

E. Light microscopy–Masson’s trichrome staining

Two resin-dentin bonded slices of each group were used for the histomorphological evaluations. Each slice was fixed in a glass holder with a photo curing adhesive (Technovit 7210 VLC, Heraeus Kulzer GmbH Co., Werheim, Germany) and ground with SiC papers of increasing fine grits (800, 1000, 1200 and 4000) in a polisher (Exakt, Apparatebau D-2000, Norderstedt, Germany) until its thickness was approximately 10 μm . Slices were stained with Masson’s trichrome for differentiation of resin and non-resin encapsulation of the exposed collagen. This dye has a high affinity for cationic elements of normally mineralized type I collagen, resulting in staining collagen green, and when demineralized, resulting in different coloration, generally red; collagen coated with adhesive stains orange and pure adhesive appears beige. Slices with adherent stained sections were dehydrated through ascending ethanol and xylene. The sections were cover slipped and examined by light microscopy (BH-2, Olympus, Tokyo, Japan) at 100 \times magnifications. Three slices were prepared from each

specimen, and images were digitalized in a scanner (Agfa Twin 1200, Agfa-Gevaert NV Mortsels, Belgium). In each specimen, the presence or absence of a red band (that would correspond to demineralized dentin) was observed. A qualitative assessment of the collagen encapsulation was completed by observing color differences within the interfacial zones of resin-dentin interfaces.

III. RESULTS AND DISCUSSION

Our results confirm that the caries-affected dentin substrata treated with a two-step self-etching adhesive doped with zinc, especially ZnO incorporated in the primer component, are remineralized after applying mechanical stimulation on the restorations.

Attained microtensile bond strength (mean and standard deviation), and nanomechanical properties (mean and standard deviation), for each group are displayed in Figures 1 and 2, respectively.

FIGURE 1

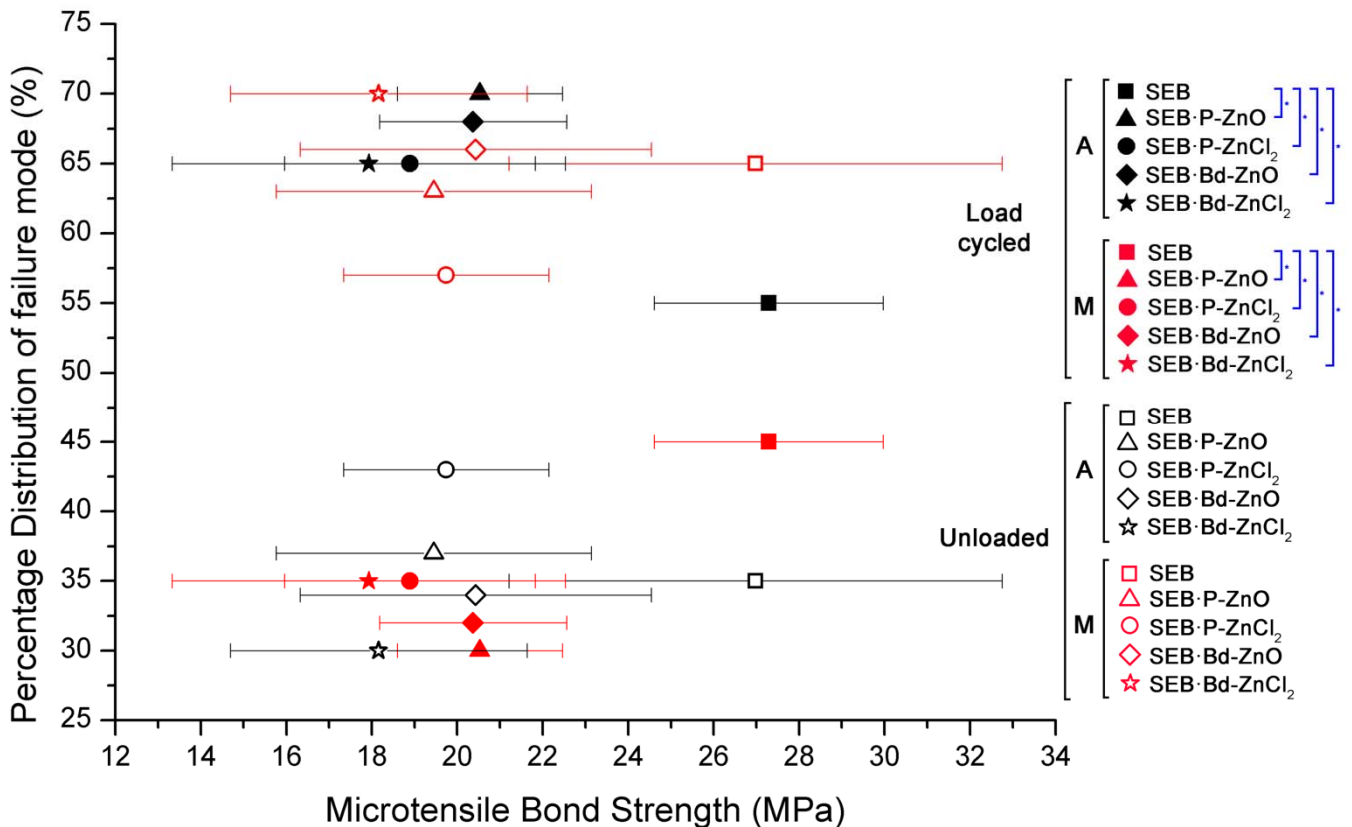


Fig 1. Microtensile bond strength values (MPa) and percentage distribution of failure mode obtained for the different experimental groups. Asterisks indicate significant difference after Student-Newman-Keuls or Student's t tests ($p < 0.05$). No differences were found between load and unloaded groups. Abbreviations: A: Adhesive failure; M: Mixed failure; SEB: SE-Bond; SEB·P: SE-Bond primer; SEB·Bd: SE-Bond bonding; ZnO: zinc oxide; ZnCl₂: zinc chloride.

FIGURE 2 (A,B)

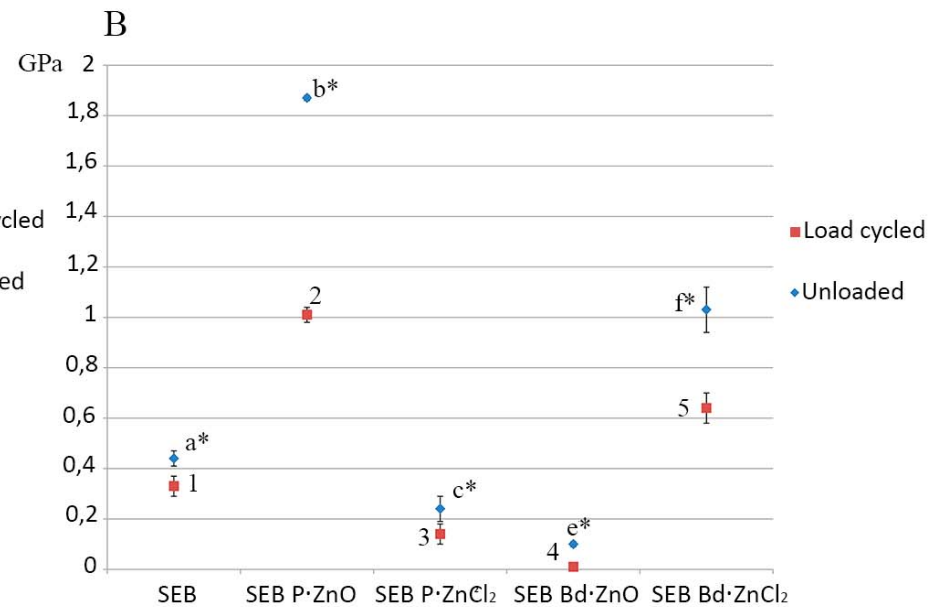
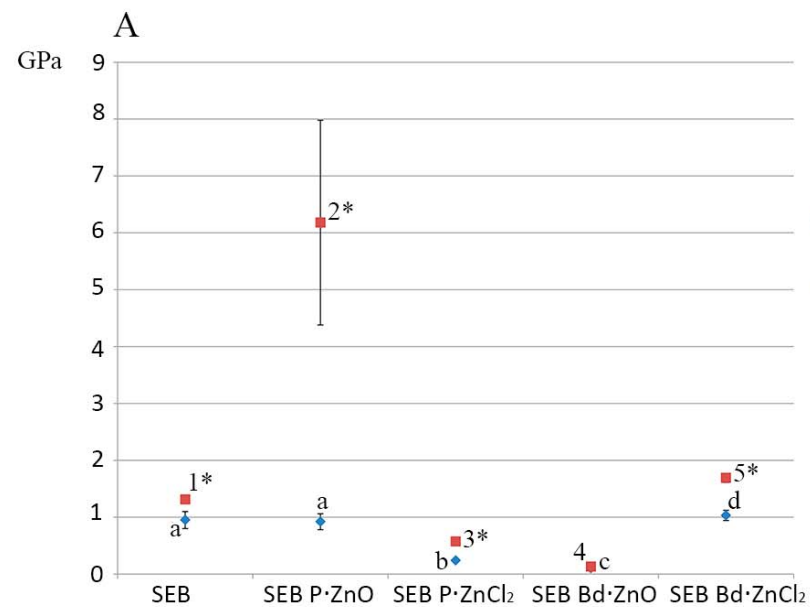


FIGURE 2 (C,D)

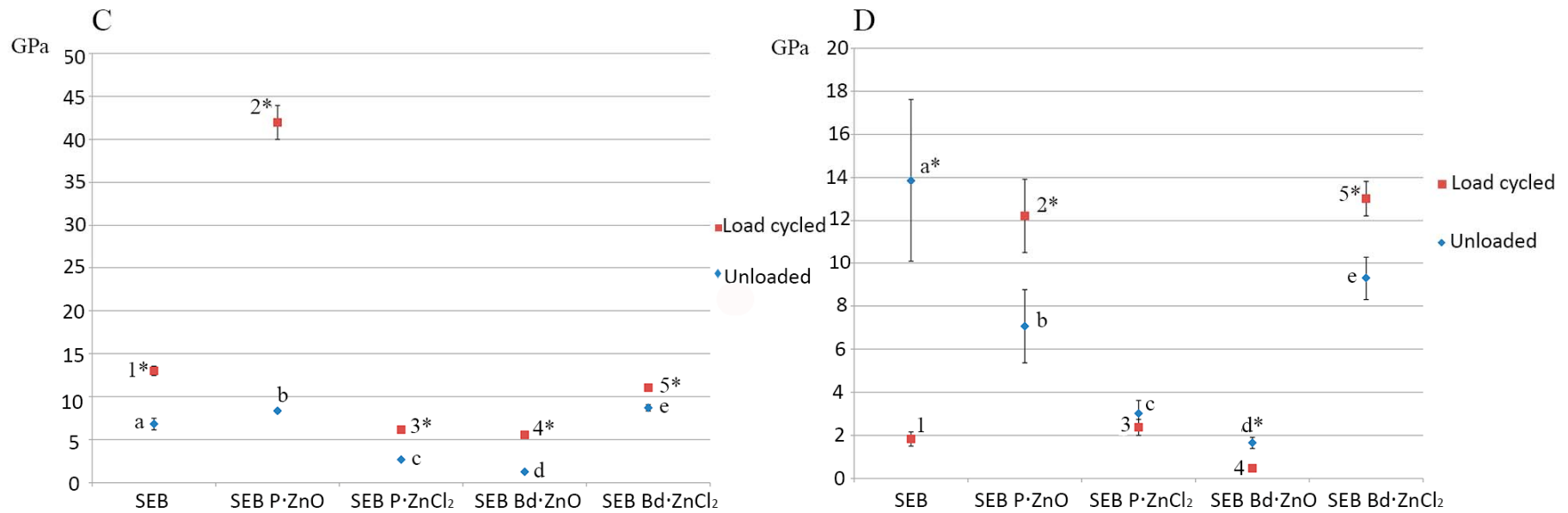


Fig 2. Mean and SD of Nanohardness (GPa) (A, B) and Young Modulus (GPa) (C, D) measured at the experimental hybrid layers (HL) and bottom of hybrid layer (BHL) in caries-affected dentin (CAD) specimens. Identical letters indicate no significant differences between unloaded restorations within the different experimental adhesives. Identical numbers indicate no significant differences between load cycled restorations within the different experimental adhesives and * indicate significant differences between unloaded and load cycled restorations within the same

experimental adhesive. Abbreviations: SEB, SE-Bond. SEB·P, SE-Bond primer. SEB·Bd: SE-Bond bonding. ZnO, zinc oxide. ZnCl₂, zinc chloride.

Raman spectroscopy-cluster results obtained at the resin-carries affected dentin interfaces are shown in Figures 3 and 4.

FIGURE 3 (I,II)

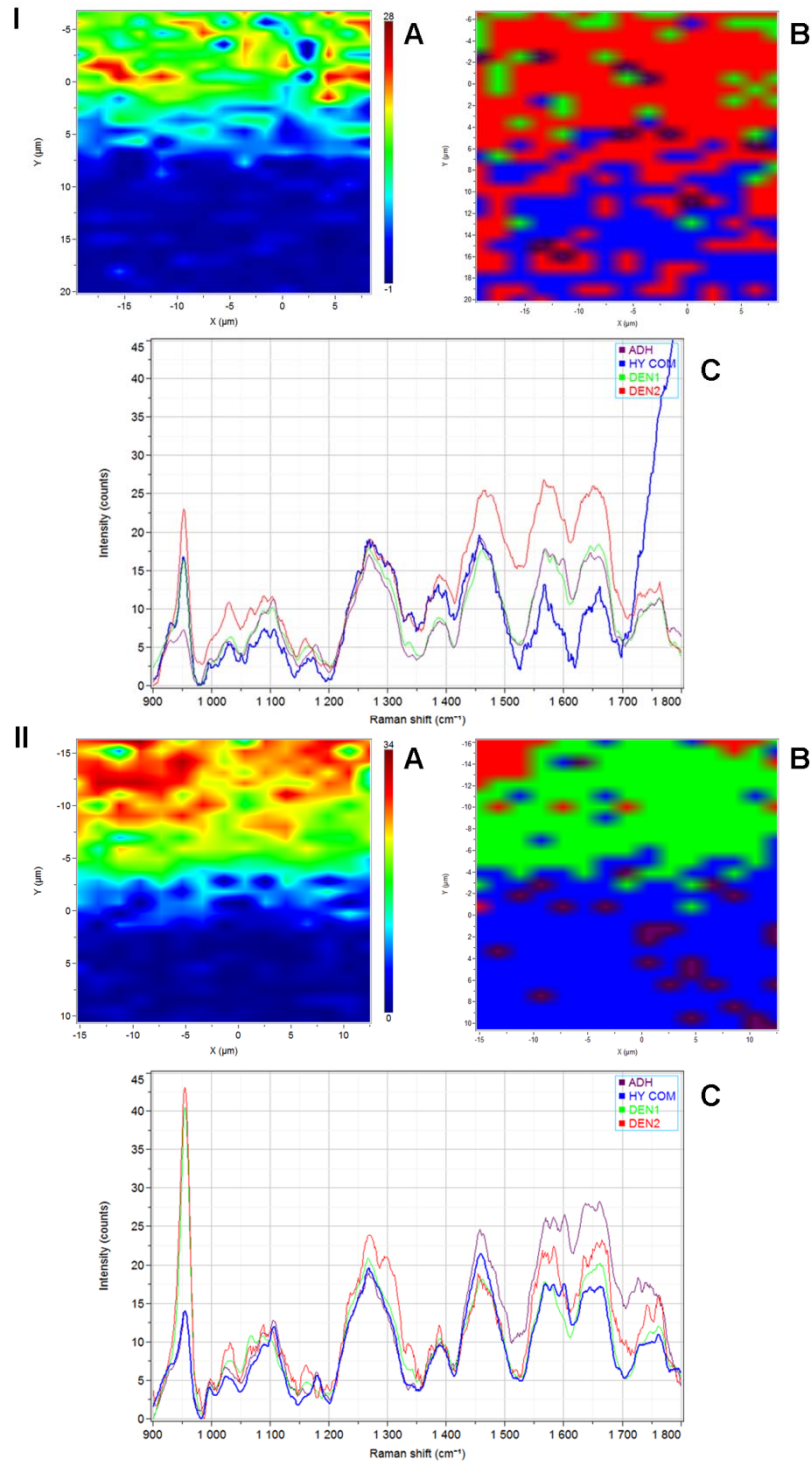


Fig 3. Bi-dimensional (2D) micro-Raman map of the phosphate peak (961 cm^{-1}) intensities (A) and K-means clustering (KMC) map of the Raman profile of the same sample (B), at the dentin-bonded interface of SEB-treated caries-affected dentin surfaces, unloaded (I), or load cycled (II). The color of the scale corresponds to the intensity of the Raman scattered light; red represents high intensity of phosphate peak and dark blue represents low intensity of phosphate peak. The plot is oriented such that the adhesive is in the lower aspect of the image and the dentin is in the upper aspect. Raman *spectra* of principal components (PCs) is also observed (C): ADH, adhesive; HY COM, hybrid complex; DEN1 and DEN2, dentin.

FIGURE 4 (I,II)

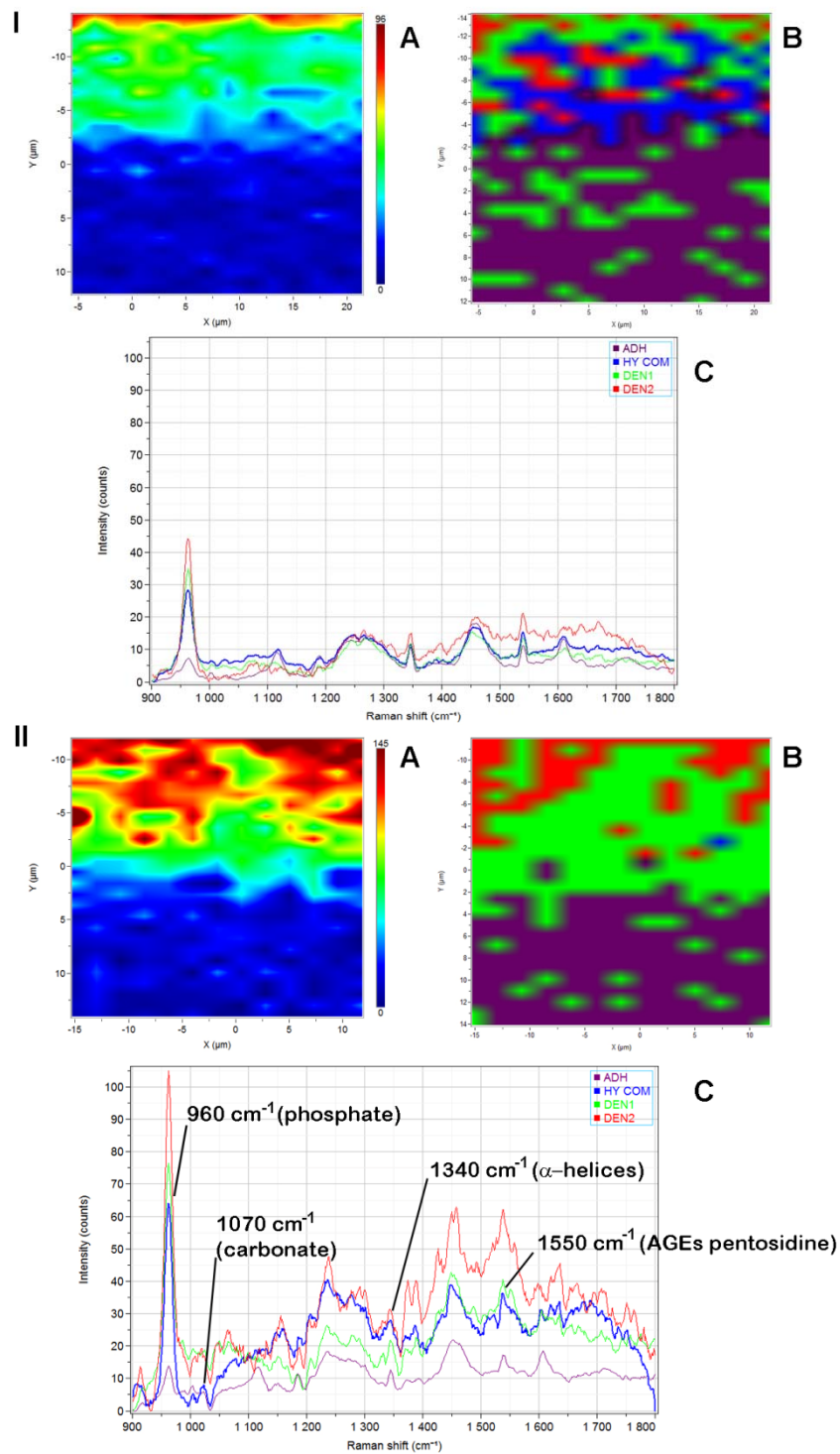


FIGURE 4 (III,IV)

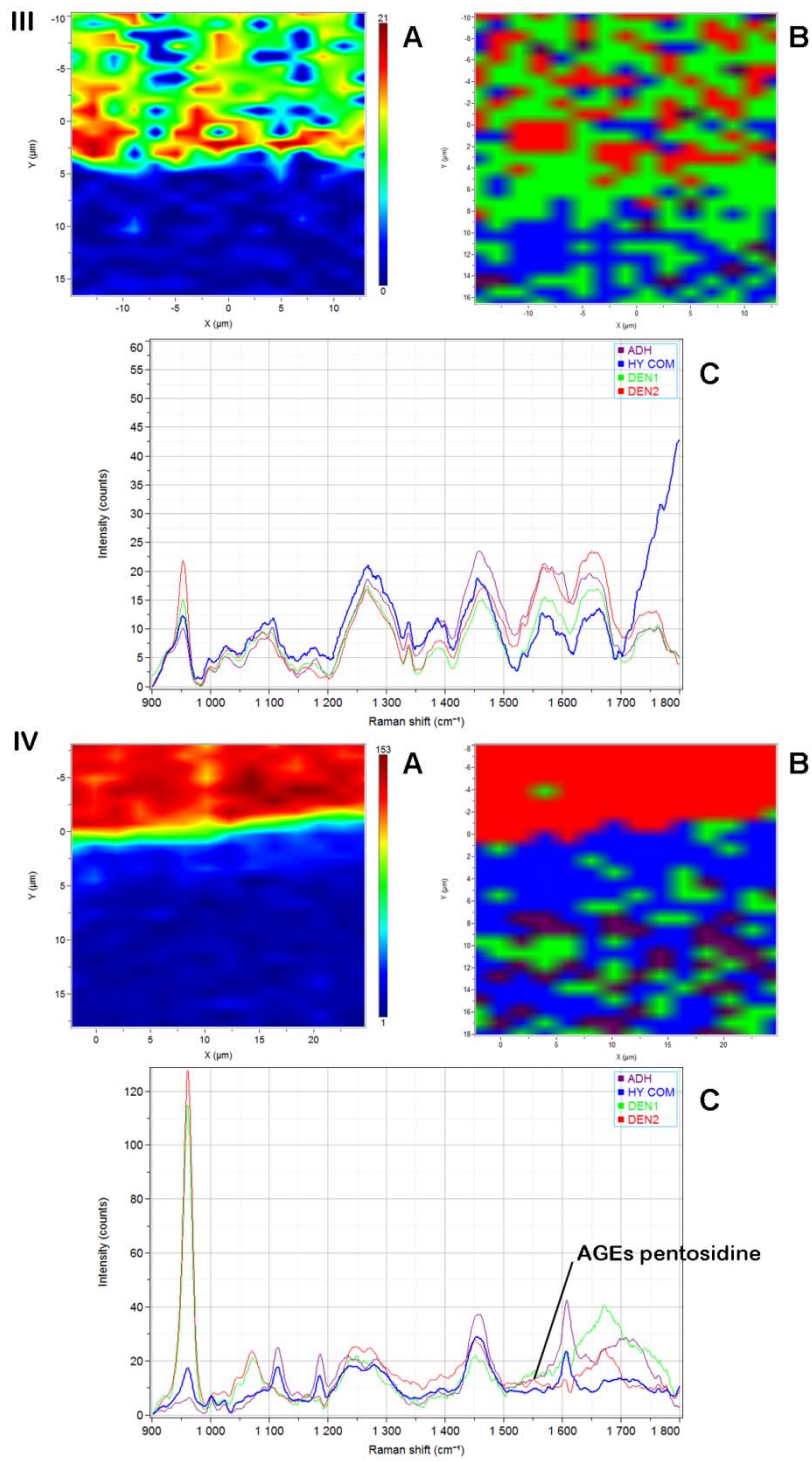


FIGURE 4 (V,VI)

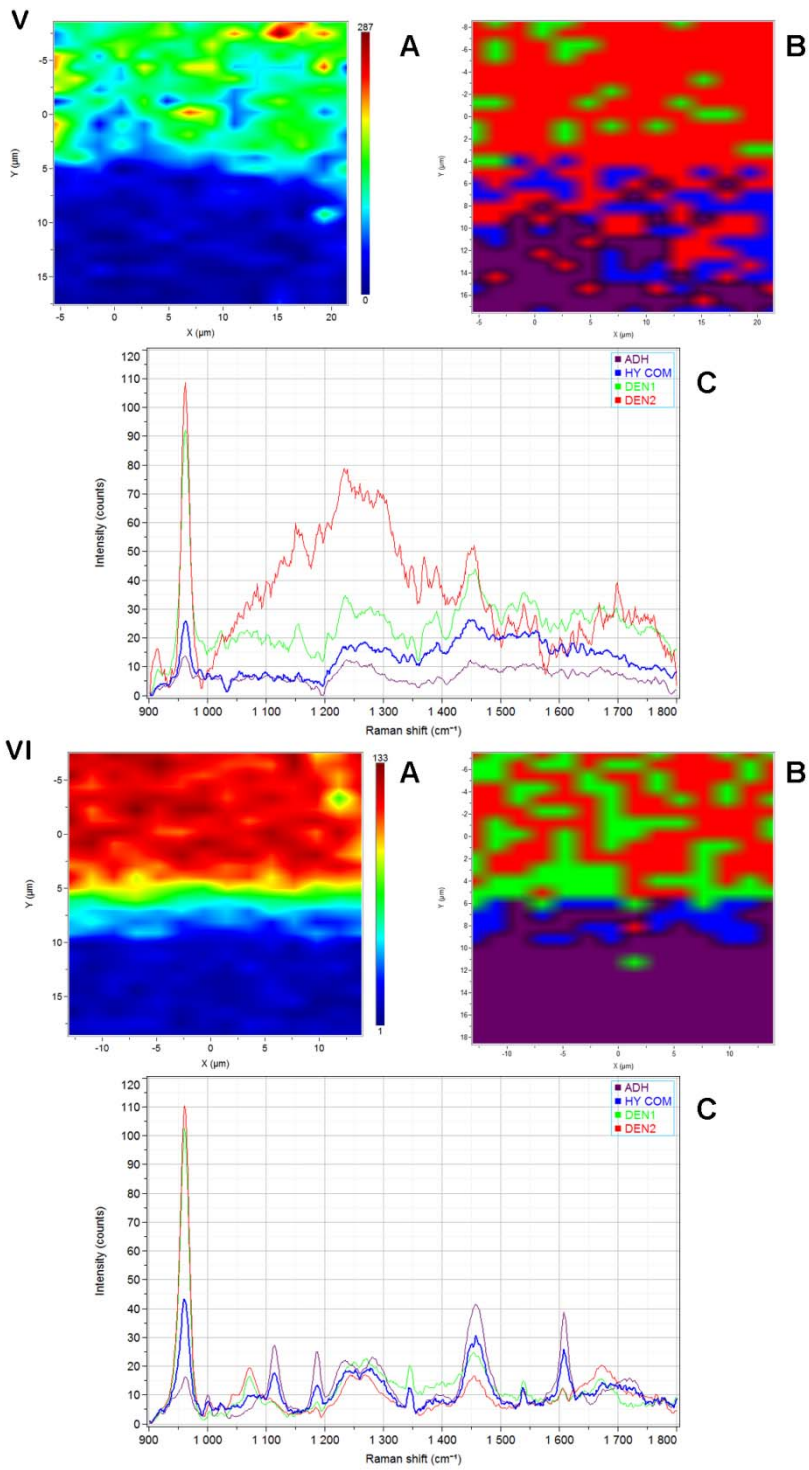


FIGURE 4 (VII, VIII)

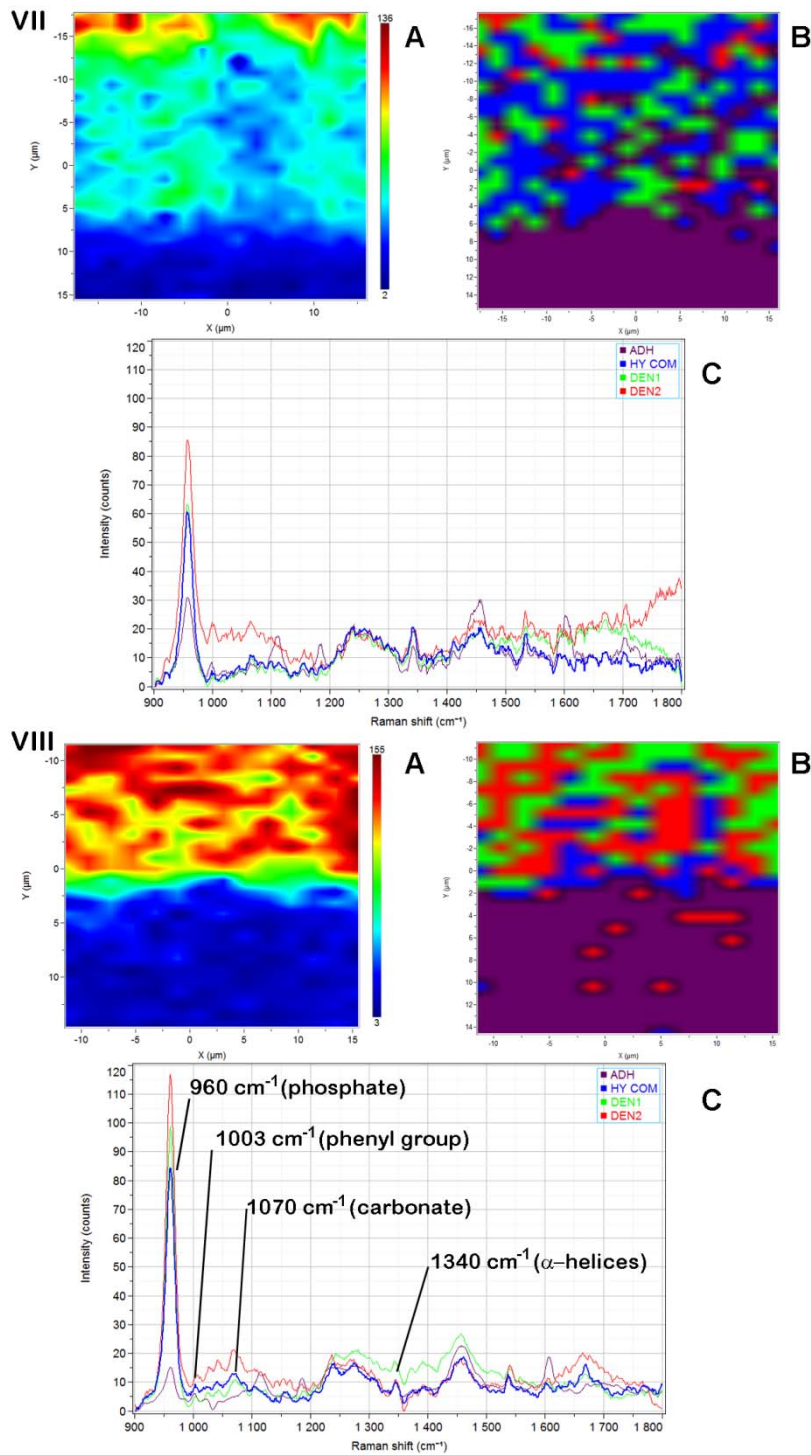


Fig 4. Bi-dimensional (2D) micro-Raman map of the phosphate peak (961 cm^{-1}) intensities (A) and K-means clustering (KMC) map of the Raman profile of the same

sample (B), at the dentin-bonded interface of SEB·P-ZnO doped unloaded (I) or load cycled (II), SEB·P-ZnCl₂ doped unloaded (III) or load cycled (IV), SEB·Bd-ZnO doped unloaded (V) or load cycled (VI), and SEB·Bd-ZnCl₂ unloaded (VII) or load cycled (VIII). The color of the scale corresponds to the intensity of the Raman scattered light; red represents high intensity of phosphate peak and dark blue represents low intensity of phosphate peak. The plot is oriented such that the adhesive is in the lower aspect of the image and the dentin is in the upper aspect. Raman *spectra* of principal components (PCs) are also observed (C): ADH, adhesive; HY COM, hybrid complex; DEN1 and DEN2, dentin.

Table II represents Raman peaks intensities/ratios of mineral, organic and adhesive components at the resin-carries affected dentin interface.

Light micrographs (Masson's trichrome) are presented in Figure 5.

FIGURE 5

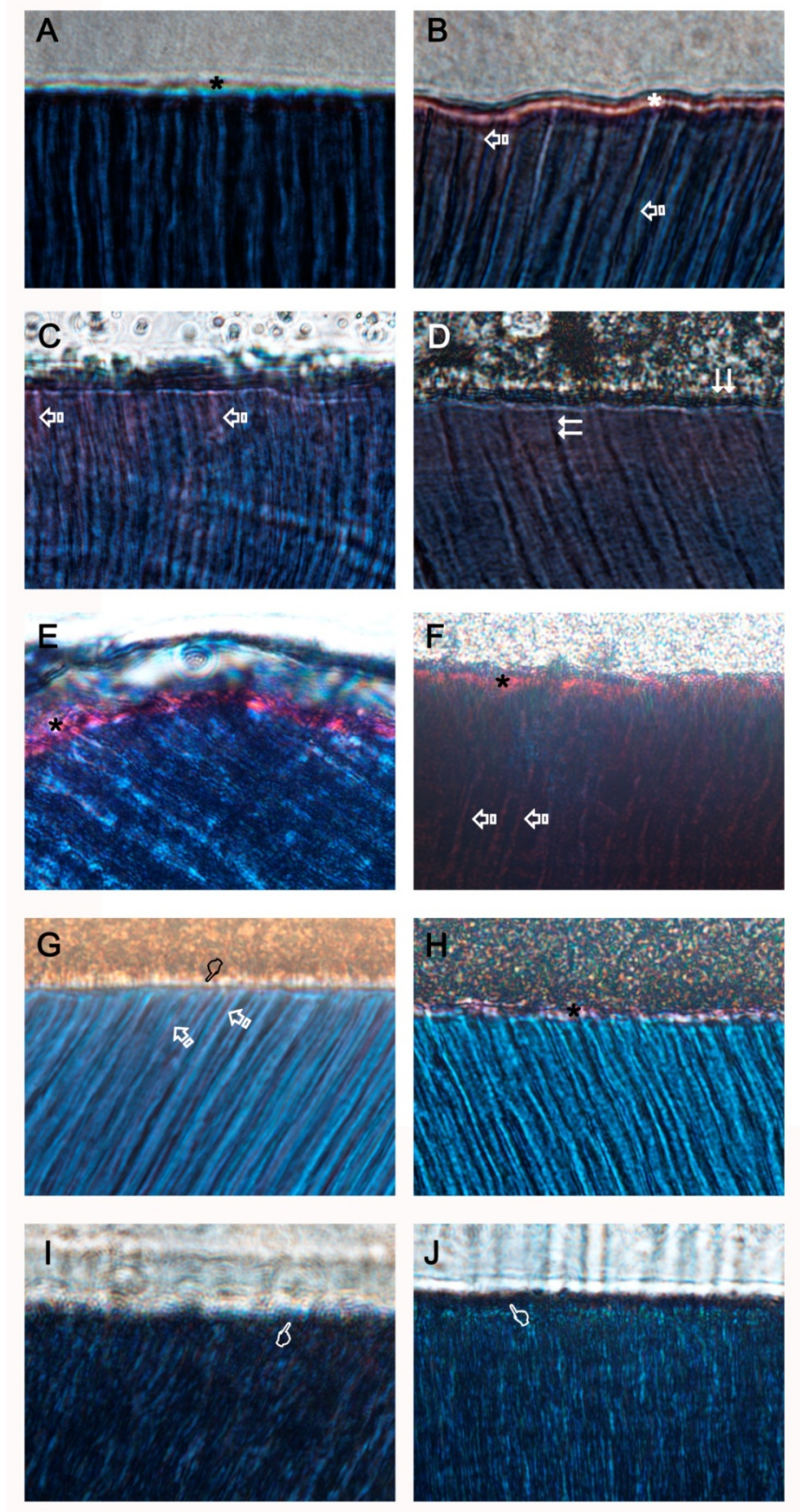


Fig 5. Representative light micrographs of SEB adhesive systems in caries-affected dentin (CAD) specimens; interfaces stained with Masson's trichrome: mineralized dentin stained green, adhesive stained beige, and exposed protein stained red. Original magnification: 150X. (A): SEB control (unloaded). (B): SEB load cycled. (C): SEB·P-ZnO unloaded. (D): SEB· P-ZnO load cycled. (E): SEB·P-ZnCl₂ unloaded. (F): SEB·P-ZnCl₂ load cycled. (G): SEB·Bd-ZnO unloaded. (H): SEB·Bd-ZnO load cycled. (I): SEB·Bd-ZnCl₂ unloaded. (J): SEB·Bd-ZnCl₂ load cycled. Limited and clear resin uncovered decalcified dentin is shown (asterisk) (A). Evidence of partial demineralization or exposed protein may be detectable at the resin-dentin interface located at both intertubular (asterisks) and peritubular (arrows) dentin areas (B, C, E, F, G, H). Slight and faint signs of demineralization show the scarce exposed proteins detected (pointers) (G, I, J). No signs of demineralization or exposed protein (red stain), *i.e.*, absence of unprotected collagen layer is detectable at the resin/dentin interface; clear observation of histological remineralization of the partially demineralized dentin layer is detected (double arrows) (D). Abbreviations: SEB, SE-Bond. SEB·P, SE-Bond primer. SEB·Bd: SE-Bond bonding. ZnO, zinc oxide. ZnCl₂, zinc chloride.

FESEM images and EDX spectra are displayed in Figures 6, 7 and 8.

FIGURE 6

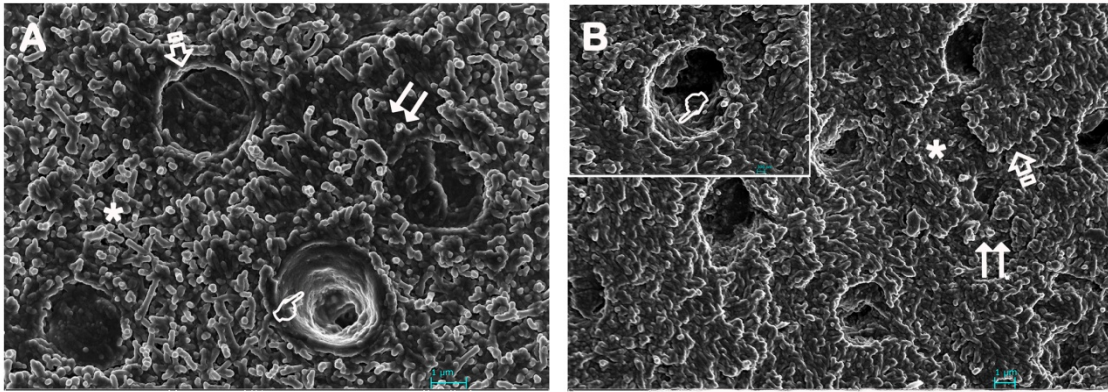


Fig 6. Field-emission scanning electron microscopy images of failures after bonding and microtensile bond strength testing. (A) SEB unloaded. (B) SEB load cycled. Mixed failures and fracture at the bottom of hybrid complex may be observed in SEB unloaded specimens (A). Collagen fibers are clearly observed at intertubular dentin, some of them partially mineralized (asterisk), or resin-infiltrated (double arrow), permitting to observe the presence of mineral crystals embedded in a remnant resin/collagen scaffold-like structure. Some non-sealed (arrow) tubules turned up mineral filled or appeared totally empty (pointer), allowing to observe the non-dissolved peritubular dentin. SEB load cycled sample (B) showed a mixed failure with the main fracture at the top of the hybridized complex. Intertubular dentin permits to observe a dense network of scales-shaped mineralized fibrils (asterisk). The mineral is covering partially (arrow) or totally (double arrow) the entrance of tubules. The prototypical D-periodicity banding of peritubular coating collagen fibrils was observed in multiple details (pointer), at high magnifications.

FIGURE 7

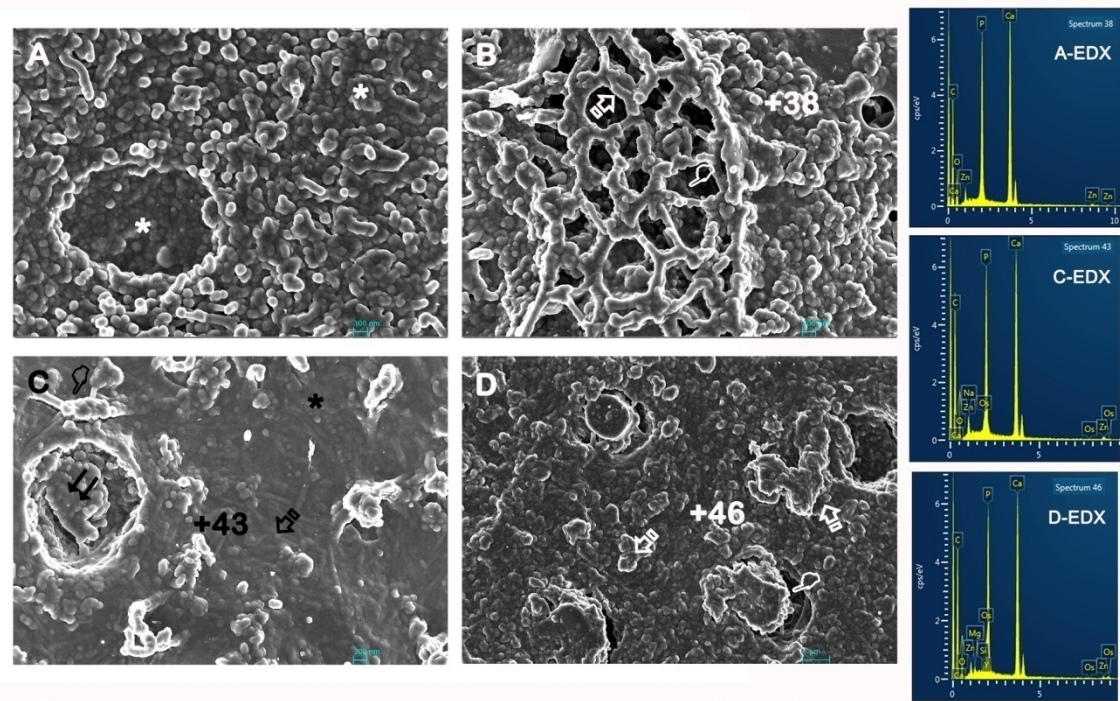


Fig 7. Field-emission scanning electron microscopy images of failures after bonding and microtensile bond strength testing (A) SEB·P-ZnO unloaded. (B) SEB·P-ZnO load cycled. (C) SEB·P-ZnCl₂ unloaded. (D) SEB·P-ZnCl₂ load cycled. SEB·P-ZnO unloaded (A) showed a mixed failure at the bottom of the hybrid complex. Multiple clumps of precipitated minerals appeared covering both intertubular and peritubular dentin (asterisks), but allowing the visual observation of tubule walls. Zinc-based salts [phosphorous (P), calcium (Ca), and zinc (Zn)] were detected in the elemental analysis (EDX, spectrum 38). When SEB·P-ZnO load cycled (B) was analyzed, a mixed failure of the hybrid complex was observable. Net-shaped precipitated crystals appeared covering the intertubular and peritubular dentin. A first layer of crystal nucleation may be detected throughout the net (pointer). Crystals nucleated coating the collagen fibrils and permitting the observation of the periodicity banding (arrow). SEB·P-ZnCl₂ unloaded (C) showed a mixed failure at the bottom of the hybrid complex. A consistent

and continuous layer of mineral is observed covering the intertubular dentin (asterisk). Mineralized collagen fibrils are noticeable below this coat of new crystals (arrow). The typical staggered pattern of those collagen fibrils, due to the characteristic D-periodicity (67 nm), is visible. Isolated mineral precipitates linked by mineralized fibers (pointer) or occupying the lumen of tubules are also observable (double arrow). Spectrum from energy dispersive analysis, attained at zone 43 is showing elemental composition of phosphorous (P), calcium (Ca) and zinc (Zn). SEB·P-ZnCl₂ load cycled (D) showed a mixed failure at the top of the hybridized complex. Failure surface analysis permitted to observe a thicker and extended platform of mineral, at intertubular dentin. These crystal formations did not allow to see the subjacent collagen fibers. Some terminal knob-like mineral structures are exhibited on the interface (arrows). Tubules appeared mineral-occupied without hermetic sealing (pointer). Spectrum from energy dispersive analysis, attained at zone 46, is showing elemental composition of phosphorous (P), calcium (Ca), magnesium (Mg) and zinc (Zn).

FIGURE 8

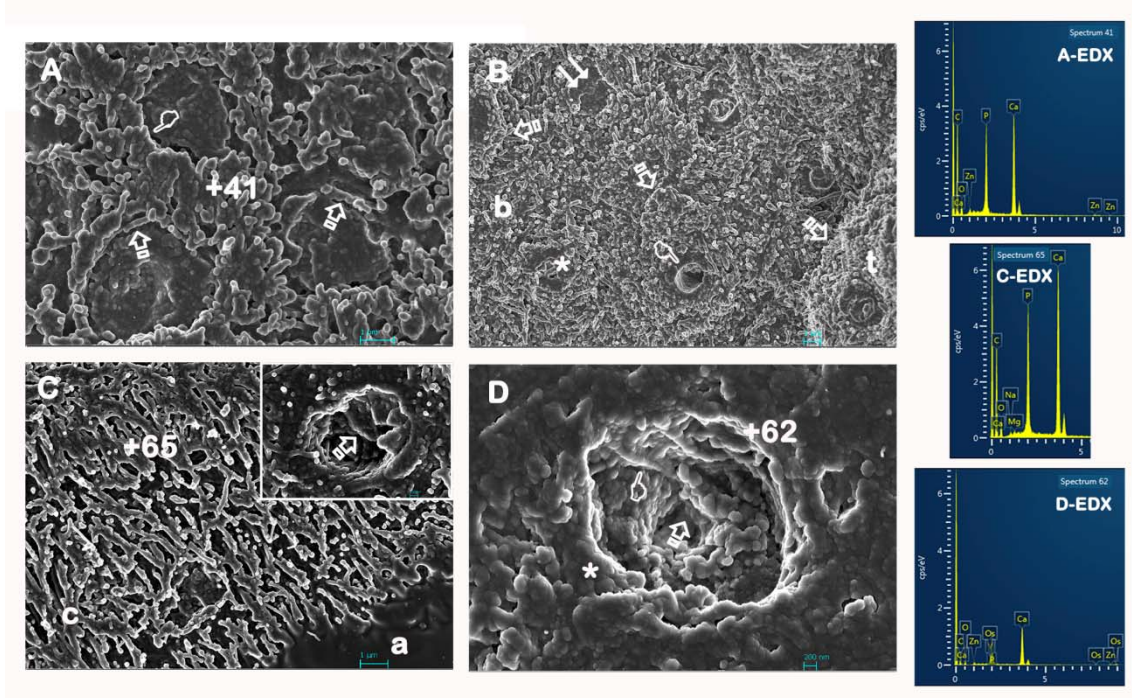


Fig 8: Field-emission scanning electron microscopy images of failures after bonding and microtensile bond strength testing. (A) SEB·Bd·ZnO unloaded. (B) SEB·Bd·ZnO load cycled. (C) SEB·Bd·ZnCl₂ unloaded. (D) SEB·Bd·ZnCl₂ load cycled. SEB·Bd·ZnO unloaded (A) produced a mixed failure at the bottom of the hybrid complex. Crystals precipitated in bigger and inter-connected knob-like formations. Collagen fibrils appeared longitudinally mineralized, rounding the entrance of tubules (arrows). Any collar of peritubular dentin was observable. Tubules were mineral-filled, forming detachment gaps (pointer). Espectrum from energy dispersive analysis, attained at zone 41, is showing elemental composition of phosphorous (P), calcium (Ca), and zinc (Zn). After using SEB·Bd·ZnO load cycled (B), a mixed failure at the bottom (b) and top (t) of the hybrid complex was present. Mineral precipitates throughout the dense network of multilayered crystals on the dentin surface were shown (arrows). Clear rings of peritubular dentin were visible (pointer). Tubules appeared hermetically (double arrow) or partially (asterisk) sealed, or mineral free with a robust peritubular dentin wall

(pointer). SEB·Bd-ZnCl₂ unloaded specimens (C) originated a mixed failure at the hybrid complex, both cohesive (c) and adhesive (a). Extensive labyrinth of crystal anastomoses below a remnant resin layer (a) were perceptible. This net like-mineral macro and microporous deposition is completely covering the dentin surface. Fibers appeared longitudinally mineralized, and the typical staggered pattern of collagen was visible at bigger magnifications (arrow). Spectrum from energy dispersive analysis, attained at zone 65, is showing elemental composition of phosphorous (P), calcium (Ca), magnesium (Mg) and zinc (Zn). (D) SEB·Bd-ZnCl₂ load cycled specimens showed a mixed failure at the top of the hybridized complex. Dentin (intertubular and peritubular) was strongly mineralized. The bulk of mineral formations only allowed a restricted display of the tubule entrances (asterisks), with precipitated in progressive strata until the complete sealing of the lumen of tubule (arrow). The characteristic D-periodicity (67 nm) was revealed (pointer). Spectrum from energy dispersive analysis, attained at zone 62, is showing elemental composition of phosphorous (P), calcium (Ca), and zinc (Zn).

Table I describes the materials and chemical used for the study.

The adhesive potential and remineralization capability of Zn-doped self-etching adhesives (SEAs) applied on caries-affected dentin (CAD) substrata have been investigated. The null hypotheses was rejected, as mechanical loading and incorporation of Zn into the chemical formulation of the adhesives did influence bond strength results. All unloaded samples performed similar (Fig 1).

The formation of ionic bonds between functional monomers and calcium may have contributed to the attained high bond strength⁴⁸. After mechanical loading,

specimens treated with un-doped SEB attained the highest bond strength values and the lowest percentage of adhesive failures (Fig 1). Strengthened of the resin-dentin interface from remineralization may have accounted for this outcome, as multiple scale-shaped precipitated of minerals were encountered deposited at the intertubular dentin, and within some of the tubules, which were totally or partially mineral-filled (Fig 6A). Nevertheless, after mechanical loading, partial demineralization or exposed collagen still remained and was detectable at the resin-dentin interface, located at both intertubular and peritubular dentin (Fig 6B). Load cycling may have produced fatigue stress expediting bonds degradation peripheral to the hybrid layer ⁴⁹. Additionally, resinous materials seems to have been degraded and extracted from the hybrid complex, increasing the porosities at the interface ⁵⁰. The loading stress which is concentrated mostly at the interface between the adhesive and the hybrid layer, and within the hybrid layer ⁵¹, may have accelerated the degradation of resin-dentin interface that was also observed with the Masson's trichrome technique (Figs 5A, 5B). Minor or null mechanical properties improvements were observed at these interfaces (Fig 2), and often limited areas of mineral precipitation were apparent (Fig 6B).

A substantial restoration of the mechanical properties of CAD tissue occurred when SEB-Zn doped adhesives were used and load cycling was applied. At the hybrid complex, specimens treated with SEB·P-ZnO after load cycling attained the highest Ei and Hi (Figs 2A, 2B). Load cycling also increased Ei at the bottom of the hybrid complex (Fig 2D) when both, SEB un-doped and SEB·Bd-ZnCl₂ were used. Replacing mineral within type I collagen is critical to restore or reestablish the normal mechanical properties of dentin ⁵². Those properties depend on the degree and on the quality of the mineralization. Indeed, the extrafibrillar minerals act as a granular material that can withstand load, but in the absence of intrafibrillar mineralization. Intrafibrillar

mineralization is the key factor to ensuring that collagen fibrils have the same high modulus of elasticity (E_i) and hardness (H_i) as occurs in natural biomineralized dentin⁵³. Therefore, the increase of E_i and H_i of the partially demineralized collagen is directly related to the precipitation of minerals at the resin-dentin interface⁵⁴, and more specifically at the intrafibrillar compartment^{53,55}, leading to functional remineralization. Functional remineralization is the result of a process that yields recovery of physical and chemical properties otherwise lost due to disease⁵².

The bonding mechanism of bonding of SEB Bond adhesive system was shown to be based upon submicron mechanical interlocking⁵⁶, supplemented by primary chemical interaction of the functional monomer MDP with hydroxyapatite (HAp) that remained around the partially exposed collagen^{57,58}. SEB involves a two-step application procedure; SEB·P represents the much more fluid and thus probably further chemically active component of SEB system, which is applied first. Most likely, the primer itself may have produced a self-assembled nano-layering⁵⁹, which consists of two MDP molecules with their methacrylate groups directed towards each other and their functional hydrogen phosphate groups directed away from each other; in between the layers calcium salts are deposited and basically hold these layers together. Zinc may causes interaction with MDP forming Zn-MDP complexes when it is combined with the primer (SEB·P-Zn doped) and applied on dentin previous to the adhesive placement (SEB·Bd), reducing the Ca-MDP salts formation⁶⁰. MDP needs to be present in a sufficiently high concentration to effectively chemically interact with HAp¹². Hence, one could speculate that the addition of other ingredients to the primer, such as ZnO or ZnCl₂ might hinder Ca-MPD salt formation, decreasing nanolayering and thus reducing the potential chemical interaction between self-etch primers and dentin. Nevertheless, both modulus of elasticity and microhardness did not change or increased, respectively,

when zinc compounds were added to SEB⁶¹. Raman analysis of the adhesive components revealed that the degree of conversion (SEB·P-ZnCl₂), the Bis-GMA penetration (SEB·P-ZnO and SEB·Bd-ZnCl₂) and the adhesive penetration (SEB·P-ZnO, SEB·Bd-ZnO, and SEB·Bd-ZnCl₂) increased in Zn-doped adhesives if compared to SEB (Table IIc).

The penetration of free MDP into the partially demineralized dentin may be compromised, due to simultaneous formation of MPD-Zn and Ca-MPD-Zn salts rather than MPD-Ca⁴⁸. Load cycling applied on dentin treated with SEB·P-ZnO promoted one of the highest increases of both nanomechanical properties (Ei, Hi), at the resin-dentin interface (Fig 2). This result corresponded with resin-dentin interfaces without any signs of demineralization or exposed protein (red stain), *i.e.*, absence of unprotected collagen layer at the resin/dentin interface (Fig 5D). FESEM images (Fig 7B) also permitted to observe a strong pattern of mineral deposition composed of zinc-based salts (Fig 7B/EDX) forming platforms or net-shaped precipitates which grew on a first layer of crystal nucleation, a mineralized matrix that contains intrafibrillar mineral oriented as found in normal dentin. Mineral remaining within the collagen fibrils could act as nuclei for regrowth of the mineral and restoration of dentin properties⁵². Mechanical loading originated the net effect, as SEB·P-ZnO unloaded produced a flatter and homogeneous model of mineral deposition in scattered clumps on peritubular and intertubular dentin (Fig 7A). The mineral phosphate and carbonate content decreased in the caries-affected region of dentin when compared with sound dentin. The mineral composition is also different from that of normal apatite due to cyclic demineralization-remineralizations¹⁸.

In the present study, the mineral growth that was observed after load cycling matched with bigger height of peaks of both phosphate (960 cm⁻¹) (PO₄⁻³, *ν1*) and carbonate (1070 cm⁻¹) (~2.25 and 1.94 fold, respectively) than in the unloaded

specimens, at the hybrid complex (HC) (Figs 4 IIA, 4 IIC). Four clusters were identified (Fig 4 IIB), corresponding to adhesive (ADH), hybrid complex (HY COM) and dentin (DEN1, DEN2). The heights of the phosphate peaks followed the trend DEN2 > DEN1 > HY COM > ADH (Fig 4 IIC). Carbonate ions are easily dissolved in the caries process, and as a consequence, its relative intensity decreases dramatically in CAD¹⁸. The increment of the carbonate band refers a rise of carbonate substitution in the lattice structure of apatite⁴⁶, and coincides with a decrease (~1.16 fold) of the gradient of mineral content (GMC), probably due to a proportional higher increase of the phosphate peak³⁸ (Fig 4 IIC). These findings also concur with an increase of crystallinity in the mineral precipitates, *i.e.*, a decrease (~1.17 fold) of full width at half maximum (FWHM) (Table IIa), respect to the unloaded specimens. FWHM expresses the crystallographic or relative atomic order, since narrower peaks suggest less structural variation in bond distances and angles³⁸; in general, the narrower the spectral peak width is, the higher the degree of mineral crystallinity³⁹. FWHM also decreased in SEB-undoped, after load cycling (Fig 3 IIC) (Table 2a). Indexes as mPPR (modified phosphate peaks ratio), *i.e.*, ratio between the mineral peak at 960 cm⁻¹ (phosphate) (PO₄³⁻) within the demineralized zone and the mineral peak (PO₄³⁻)⁴⁰ within the caries affected substratum, and RMC (relative mineral concentration), *i.e.*, mineral-to-matrix ratio did also augment (~2.69 and 2.24 fold, respectively) after load cycling. Therefore, mechanical loading contributed to an increase of phosphate peaks and a decrease of peaks at phenyl group (1003 cm⁻¹) (Table IIb). This quotient promoted the higher RMC which was attained in dentin treated with SEB·P-ZnO. Raman analysis of the organic components showed lower collagen crosslinking at the interface, after applying load cycling, in both SEB·P-ZnO and SEB·P-ZnCl₂ groups. Declined crosslinking of collagen usually results after nucleation. Only AGEs-pentosidine (1550 cm⁻¹)

augmented in those groups (~3.41 and 1.45 fold, respectively) (Figs 4 IIC, 4 IVC). Tang and Vashishth (2010),⁶² have stated that an increase of AGE crosslink induces a marked decrease in the propagation fracture toughness, in bone. The ratios which reflect the nature of collagen increased, in general, at the hybrid complex after load cycling, confirming recovery, better organization, improved structural differences and collagen quality^{30,43,46}.

Table IIa. Mineral components in SEB-treated caries affected dentin surfaces.

			Relative Presence of Mineral				FWHM	GMC Ratio C/P	mPPR Ratio phosphate peak /caries-affected substratum
			Phosphate [961]			Carbonate [1070]			
			Peak	Area	RMC	Peak	Phosphate		
SEB	Control	ADH	7.24	206.12	2.07	5.38	35.69	0.74	0.06
		HC	16.79	477.1	5.54	6.6	22.57	0.39	0.15
		DEN1	16.47	404.18	5.66	7.02	19.34	0.43	0.14
		DEN2	23.02	564.86	3.94	10.15	19.34	0.44	0.20
	Load cycled	ADH	13.65	335.56	2.77	9.2	19.33	0.67	0.12
		HC	14.42	354.9	3.56	10.1	19.33	0.70	0.13
		DEN1	40.78	1161.25	9.60	11.05	22.56	0.27	0.35
		DEN2	45.29	1289.67	8.66	14.41	22.56	0.32	0.39
SEB·P-ZnO	Control	ADH	7.29	236.7	6.39	2.61	25.73	0.36	0.06
		HC	28.59	816.66	4.40	8.38	22.51	0.29	0.25
		DEN1	35.1	864.19	6.25	6.86	19.30	0.20	0.31
		DEN2	44.35	1091.91	38.90	6.12	19.30	0.14	0.39
	Load cycled	ADH	13.89	341.5	1.80	7.26	19.27	0.52	0.12
		HC	64.25	1580.1	11.85	16.25	19.28	0.25	0.56
		DEN1	76.58	1883.34	3.98	21.52	16.09	0.28	0.67
		DEN2	105.1	2168.1	6.20	25.13	19.27	0.24	0.91
SEB·P-ZnCl ₂	Control	ADH	10.13	288.16	3.10	6.16	22.56	0.61	0.09
		HC	12.32	397.38	2.49	8.34	25.79	0.68	0.11
		DEN1	15.13	371.51	4.90	7.89	19.34	0.52	0.13
		DEN2	21.9	537.54	6.24	8.7	19.34	0.40	0.19
	Load cycled	ADH	6	171.36	0.99	5.29	22.52	0.88	0.05
		HC	19.41	629.75	1.96	6.14	25.72	0.32	0.17
		DEN1	115.05	2828.55	22.69	21.41	19.30	0.19	1.00
		DEN2	127.48	3139.38	15.62	23.7	19.34	0.19	1.11
SEB·Bd-ZnO	Control	ADH	13.77	446.59	2.02	6.62	25.72	0.48	0.12
		HC	26	639.88	3.32	6.9	19.29	0.27	0.23
		DEN1	92.18	2270.9	9.78	22.74	19.33	0.25	0.80
		DEN2	108.72	2244.01	7.06	32.52	16.10	0.30	0.94
	Load cycled	ADH	16.47	535	1.59	5.54	25.77	0.34	0.14
		HC	44.35	1267.2	5.56	10.47	22.55	0.24	0.39
		DEN1	105.38	2176.33	22.05	17.25	16.11	0.16	0.92
		DEN2	112.05	2764.32	15.43	20.1	19.37	0.18	0.97
SEB·Bd-ZnCl ₂	Control	ADH	31.01	884.7	3.58	8.47	22.58	0.27	0.27
		HC	60.69	1728.41	10.95	11.09	22.53	0.18	0.53
		DEN1	63.52	1562.47	16.41	10.12	19.35	0.16	0.55
		DEN2	85.72	2445.67	3.82	22.94	22.58	0.27	0.75
	Load cycled	ADH	15.4	379.18	2.52	5.06	19.31	0.33	0.13
		HC	84.58	2082.66	8.88	3.17	19.32	0.04	0.74
		DEN1	98.72	2036.83	18.66	10.9	16.10	0.11	0.86
		DEN2	116.84	2876.81	9.45	21.27	19.32	0.18	1.02

Abbreviations: ADH: Adhesive; HC: HY COM or Hybrid complex; DEN1, DEN 2: Dentin; RMC: Relative Mineral Concentration between mineral/Phenyl (1003); FWHM: Full-width half-maximum; GMC: Gradient in Mineral Content; mPPR: modified Phosphate Peaks Ratio. Peaks positions are expressed in cm⁻¹.

Table IIb. Organics components in SEB-treated caries affected dentin surfaces.

			Norma- lization	Crosslinking				Nature of collagen								
			Phenyl [1003]	Pyrid. [1032]	Ratio 1031/1001	Ratio phenyl/CH ₂ [1003/CH]	AGEs- Pentosidine [1550]	A-III [1246- 1270]	CH ₂ [1450]	A-I [1655- 1667]	Ratio Amide I/ Amide III	Ratio Amide III/ CH ₂	Ratio Amide I/ CH ₂	Ratio Amide III/ AGEs- Pentosidine	Ratio Amide I/ AGEs- Pentosidine	α - helices [1340]
SEB	Control	ADH	3.5	5.76	1.65	0.18	11.68	17.93	19.22	16.83	0.94	0.93	0.88	1.54	1.44	4.00
		HC	3.03	5.61	1.85	0.16	7.33	19.06	19.23	12.99	0.68	0.99	0.68	2.60	1.77	9.57
		DEN1	2.91	6.37	2.19	0.17	11.61	17.98	17.59	18.44	1.03	1.02	1.05	1.55	1.59	5.64
		DEN2	5.85	10.85	1.85	0.23	21.28	19.13	25.51	25.27	1.32	0.75	0.99	0.90	1.19	9.11
	Load cycled	ADH	4.92	6.38	1.30	0.20	11.11	18.86	24.56	28.19	1.49	0.77	1.15	1.70	2.54	4.59
		HC	4.05	5.60	1.38	0.18	5.59	20.14	21.96	17.71	0.88	0.92	0.81	3.60	3.17	4.83
		DEN1	4.25	7.76	1.83	0.23	5.78	21.12	18.39	20.48	0.97	1.15	1.11	3.65	3.54	6.66
		DEN2	5.23	12.08	2.31	0.25	19.94	26.06	21.03	25.40	0.97	1.24	1.21	1.31	1.27	10.38
SEB·P-ZnO	Control	ADH	1.14	2.11	1.85	0.06	6.13	13.75	18.17	5.37	0.39	0.76	0.30	2.24	0.88	10.90
		HC	6.50	5.85	0.90	0.38	9.19	14.56	17.03	11.14	0.77	0.85	0.65	1.58	1.21	11.64
		DEN1	5.62	4.62	0.82	0.36	8.89	13.46	15.59	8.48	0.63	0.86	0.54	1.51	0.95	11.97
		DEN2	1.14	1.02	0.89	0.06	16.11	16.23	20.22	18.79	1.16	0.80	0.93	1.01	1.17	15.09
	Load cycled	ADH	7.73	0.17	0.02	0.35	13.37	16.09	21.91	11.78	0.73	0.73	0.54	1.20	0.88	12.88
		HC	5.42	2.62	0.48	0.14	31.3	36.66	38.94	34.36	0.94	0.94	0.88	1.17	1.10	28.13
		DEN1	19.26	12.47	0.65	0.45	37.79	23.45	42.87	26.54	1.13	0.55	0.62	0.62	0.70	21.92
		DEN2	16.96	8.47	0.50	0.27	54.63	35.36	63.00	39.51	1.12	0.56	0.63	0.65	0.72	31.51
SEB·P- ZnCl ₂	Control	ADH	3.27	4.99	1.53	0.14	21.39	18.63	23.53	18.52	0.99	0.79	0.79	0.87	0.87	9.31
		HC	4.94	6.09	1.23	0.26	8.21	21.08	18.78	13.65	0.65	1.12	0.73	2.57	1.66	11.23
		DEN1	3.09	5.73	1.85	0.20	10.11	17.44	15.11	17.02	0.98	1.15	1.13	1.73	1.68	6.78
		DEN2	3.51	6.61	1.88	0.22	16.61	16.90	16.28	23.51	1.39	1.04	1.44	1.02	1.42	7.20
	Load cycled	ADH	6.06	0.27	0.04	0.16	13.5	20.25	36.99	24.52	1.21	0.55	0.66	1.50	1.82	3.92
		HC	9.89	2.78	0.28	0.23	15.23	21.32	43.78	11.48	0.54	0.49	0.26	1.40	0.75	11.60
		DEN1	5.07	4.03	0.79	0.23	16.72	19.52	22.25	40.79	2.09	0.88	1.83	1.17	2.44	6.02
		DEN2	8.16	6.90	0.85	0.29	13.1	24.97	27.90	24.70	0.99	0.89	0.89	1.91	1.89	12.47
SEB·Bd- ZnO	Control	ADH	6.82	1.40	0.21	0.55	11.03	12.05	12.40	9.90	0.82	0.97	0.80	1.09	0.90	5.30
		HC	7.82	1.28	0.16	0.30	22.07	18.86	26.37	16.40	0.87	0.72	0.62	0.85	0.74	14.42
		DEN1	9.43	20.46	2.17	0.18	23.33	71.18	52.14	32.34	0.45	1.37	0.62	3.05	1.39	45.23
		DEN2	15.41	16.67	1.08	0.35	33.03	29.43	44.17	31.03	1.05	0.67	0.70	0.89	0.94	20.65
	Load cycled	ADH	10.37	2.10	0.20	0.25	7.43	20.50	42.07	12.58	0.61	0.49	0.30	2.76	1.69	12.97
		HC	7.98	6.60	0.83	0.25	8.62	19.41	31.98	15.50	0.80	0.61	0.48	2.25	1.80	13.77
		DEN1	4.78	2.40	0.50	0.19	9.8	23.35	25.36	16.39	0.70	0.92	0.65	2.38	1.67	20.63
		DEN2	7.26	4.77	0.66	0.41	8.13	17.38	17.60	20.72	1.19	0.99	1.18	2.14	2.55	12.95
SEB·Bd- ZnCl ₂	Control	ADH	8.65	5.20	0.60	0.29	12.33	18.64	30.30	12.17	0.65	0.62	0.40	1.51	0.99	14.21
		HC	5.54	5.45	0.98	0.27	13.53	20.23	20.46	12.12	0.60	0.99	0.59	1.50	0.90	20.89
		DEN1	3.87	4.11	1.06	0.19	19.15	17.98	19.96	23.37	1.30	0.90	1.17	0.94	1.22	19.42
		DEN2	22.46	2.06	0.09	0.96	18.63	20.03	23.44	25.93	1.29	0.85	1.11	1.08	1.39	20.15
	Load cycled	ADH	6.10	0.52	0.09	0.27	8.67	15.58	22.75	9.49	0.61	0.68	0.42	1.80	1.09	11.08
		HC	9.52	7.42	0.78	0.51	8.37	16.74	18.65	16.23	0.97	0.90	0.87	2.00	1.94	10.04
		DEN1	5.29	5.57	1.05	0.20	9.67	20.83	26.84	12.84	0.62	0.78	0.48	2.15	1.33	17.38
		DEN2	12.37	13.77	1.11	0.68	10.5	18.03	18.06	20.23	1.12	1.00	1.12	1.72	1.93	10.88

Abbreviations: ADH: Adhesive; HC: HY COM or Hybrid complex; DEN1, DEN 2: Dentin; A: Amide; Pyrid: Pyridinium; AGEs: Advanced glycation end products. Peaks positions are expressed in cm⁻¹.

Table IIc. Adhesive components in SEB-treated caries affected dentin surfaces

			Degree of Adhesive Presence				
			DC [1637/1608]	Bis-GMA Penetration [1113/A-I]	Adhesive Penetration [1453/1667]	Carbonyl Group [1720]	CH ₂ def [1453]
SEB	Control	ADH	0.93	0.67	1.14	9.97	19.22
		HC	0.95	0.56	1.48	17.59	19.23
		DEN1	4.42	0.55	0.95	8.98	17.59
		DEN2	2.21	0.46	1.01	12.06	25.51
	Load cycled	ADH	1.30	0.45	0.87	18.29	24.56
		HC	1.33	0.70	1.24	10.07	21.96
		DEN1	1.73	0.42	0.90	9.65	18.39
		DEN2	1.47	0.49	0.83	13.15	21.03
SEB·P-ZnO	Control	ADH	0.52	6.31	3.38	7.60	18.17
		HC	0.78	0.92	1.53	10.69	17.03
		DEN1	0.83	0.73	1.84	7.06	15.59
		DEN2	1.05	0.23	1.08	13.53	20.22
	Load cycled	ADH	0.62	1.15	1.86	12.24	21.91
		HC	1.21	0.55	1.13	28.45	38.94
		DEN1	1.08	0.64	1.62	22.15	42.87
		DEN2	1.29	0.41	1.59	31.94	63
SEB·P-ZnCl ₂	Control	ADH	1.36	6.31	1.27	9.03	23.53
		HC	1.97	0.87	1.38	15.49	18.78
		DEN1	1.82	0.37	0.89	8.47	15.11
		DEN2	1.48	0.22	0.69	11.38	16.28
	Load cycled	ADH	0.52	1.00	1.51	27.65	36.99
		HC	0.36	1.65	3.81	13.8	43.78
		DEN1	1.34	0.19	0.55	26.09	22.25
		DEN2	1.33	0.40	1.13	10.92	27.9
SEB·Bd-ZnO	Control	ADH	1.25	0.63	1.25	6.17	12.4
		HC	1.00	0.38	1.61	11.55	26.37
		DEN1	1.63	1.22	1.61	31.01	52.14
		DEN2	1.35	0.59	1.42	24.88	44.17
	Load cycled	ADH	0.29	2.19	3.34	15.65	42.07
		HC	0.42	1.15	2.06	13.01	31.98
		DEN1	0.93	0.47	1.55	6.77	25.36
		DEN2	1.31	0.39	0.85	11.83	17.6
SEB·Bd-ZnCl ₂	Control	ADH	0.56	1.46	2.49	14.09	30.3
		HC	0.89	0.71	1.69	8.16	20.46
		DEN1	1.11	0.26	0.85	17.75	19.96
		DEN2	1.27	0.56	0.90	22.88	23.44
	Load cycled	ADH	0.41	1.44	2.40	9.04	22.75
		HC	1.30	0.45	1.15	6.85	18.65
		DEN1	0.88	0.59	2.09	5.03	26.84
		DEN2	1.48	0.67	0.89	12.21	18.06

Abbreviations: ADH: Adhesive; HC: HY COM or Hybrid complex; DEN1, DEN 2: Dentin; DC: Degree of conversion of adhesive; Bis-GMA: bisphenol A diglycidyl methacrylate.

Peaks positions are expressed in cm⁻¹.

Peaks at 1340 cm^{-1} (α -helices) also augmented, denoting a greater sensitivity to molecular orientation in order to enhance further crystallization⁴⁴, as mineral nucleation is more advanced in comparison with the SEB·P-ZnCl₂ group (Table IIa). Nevertheless, the ratios A-III and I/AGES-Pentosidine decreased in both SEB·P-ZnO and SEB·P-ZnCl₂, as an inversely proportional increase of the peaks at 1550 cm^{-1} (AGES-Pentosidine), was measured (Table IIb). This indicates a lower collagen scaffolding characteristic, *i.e.*, decreased ratio A-III/AGES-Pentosidine strengthen the advanced degree of mineral precipitation. The increase of collagen maturation has been also associated with a dose-dependent increase of pentosidine that was correlated with bone turnover rate⁶³.

When dentin was treated with SEB·Bd-ZnCl₂, remineralization at the bonding interface below the resin-primed demineralized collagen was produced even with presence of a previous primer layer (SEB·P). These Ca-MDP complexes were organized in nano-layering⁵⁹, forming an extensive labyrinth of macro and microporous crystal anastomoses among elongated calcified nucleus (Fig 8C). This net like-mineral deposition completely covered the dentin surface, and did not hamper the inward diffusion of ions, helping for further interactions between the remaining Ca and Zn ions, the curable resin matrix containing acidic functional, Zn-MPD and Ca-MPD-Zn complexes, and the partially demineralized collagen. EDX spectra performed at load cycled specimens treated with SEB·Bd-ZnCl₂ presented elemental composition of phosphorous (P), calcium (Ca), zinc (Zn), and magnesium (Mg) (Fig 8C-EDX). Similar EDX analysis was attained from specimens treated with SEB·P-ZnCl₂ after load cycling (Fig 7D-EDX). The magnesium ion is known to have a significant effect on remineralization processes⁶⁴. The hydroxyapatite crystallites contain Mg²⁺, which substitutes for Ca²⁺⁶⁴. The destabilizing effect of Mg is attributable to the markedly

smaller ionic radius of Mg^{2+} (0.65 Å) in comparison with Ca^{2+} (0.99 Å); substitution of the smaller sized ion gives rise to lattice strain, which favors the hydroxyapatite-whitlockite transition. The high content of Mg is thought to reflect a high measure of re-precipitation of Mg as β -tricalcium phosphate $[(\text{Ca},\text{Mg})_3(\text{PO}_4)_2]$ (whitlockite)^{65,66}, less soluble than hydroxyapatite at $\text{pH} < 5.5$ ¹⁸. Mg-substituted β -tricalcium phosphate may have formed in the dentinal tubules as a result from an increase in the Mg/Ca in the medium⁶⁷, contributing to enhance mechanical properties of dentin⁶⁸. The caries process consists of a dynamic process of dissolution of the dentin mineral (apatite) and remineralization. When the remineralization process is slower than the dissolution process, the caries lesion progresses. When remineralization is faster than the dissolution process, the development of the caries lesion is slowed down or even arrested. In such cases, precipitation of large whitlockite crystals occurs in the tubules after the cell processes have withdrawn. Although the relatively low amount of Mg detected in Fig 8C-EDX does not support the existence of whitlockite in the area, the relative low Mg/Ca ratio leads to this conclusion^{69,70}.

An increase of calcium concentration is produced at the demineralized dentin and beneath the resin-dentin interface⁷¹; as a result, new Ca-MDP salts are formed and greater Ei values are produced at the bottom of the hybrid complex in specimens of CAD treated with SEB·Bd-ZnCl₂ after load cycling (Fig 2D). Nevertheless, resin-dentin interfaces revealed some limited signs of demineralization (Fig 5J) when specimens treated with SEB·Bd-ZnCl₂ were load cycled. This compromised interface contributed to produced a progressive increase of carboxy terminal telopeptide of type I collagen (ICTP), possibly because of, *i*) hydrolytic resin degradation that will lead to exposed unprotected collagen⁷², and *ii*) this major proteolytic degradation may be a result of a restricted formation of MDP-Ca salts caused by Zn^{2+} interactions with 10-MDP. MDP-

Ca may also act as a Zn chelator and Zn-MDP-Ca complexes may reduce Ca-MDP salt formation. Similarly, an over-etching effect produced by ZnCl₂ has been advocated as a secondary source of this instability; ZnCl₂ is highly acidic⁷³, soluble, and hydrophilic, rapidly diffusing through the smear layer thereby demineralizing the underlying dentin²¹. At FESEM evaluation, intertubular and peritubular dentin appeared strongly mineralized, with organized plate-like crystals deposited at intertubular spaces, with tubules nearly filled, conducting normally until the complete sealing of tubule. The typical staggered pattern of some collagen fibrils, closely resembling those in noncarious dentin¹⁸ and due to the characteristic 67 nm D- periodicity, was visibly remineralized (Fig 8D). This strong crystal growing suggests that new mineral was deposited within the intrafibrillar and extrafibrillar portions of the matrix⁵². Both unloaded and load cycling specimens of CAD treated with SEB·Bd-ZnCl₂ showed two typical phases of CAD formation, which consisted on occlusion of tubules by fine, granular or amorphous materials, and by narrowing of the tubule lumen concomitant with a thickening of peritubular dentin⁶⁷. The energy-dispersive analysis demonstrated the presence of phosphorous (P), calcium (Ca), and zinc (Zn) in these precipitates (Fig 8D-EDX). Raman analysis displayed the formation of four clusters, clearly delimited (Fig 4 VIIIB), which distributed according to variances associated for data differentiation, *i.e.*, DEN1 and DEN2 at the top, ADH, at the bottom and HY COM in the middle, the three main component conforming the resin-caries affected dentin interface. This new mineral formation showed, after load cycling, *i*) bigger height of peak and area of phosphate (960 cm⁻¹) (~1.39 and 1.20 fold, respectively) than the unloaded specimens, *ii*) an increase of crystallinity (~1.39 decrease of FWHM), possibly influenced by the higher Mg content⁶⁴ (Figs 4 VIIIA, 4 VIIC). And *iii*) a decrease (~4.5 fold) of the gradient of mineral content (GMC), as a result of a lowering

(~3.50 fold) of carbonate substitution in the lattice structure of apatite ⁴⁶ (Table IIa). Similarly, the modified phosphate peaks ratio (mPPR) also raised (~1.40 fold). Nevertheless, the relative mineral concentration (RMC) decreased (~1.23 fold), as the aromatic ring of phenylalanine residues in collagen (phenyl group), at 1003 cm⁻¹ also increased (Fig 4 VIIC). This remineralization effect conducted to observe faint signs of dentin demineralization, *i.e.*, detection of scarce exposed collagen (Fig 5J). The ratios which support the nature of collagen, as Amide I/Amide III, Amide I/CH₂, A-III and I/AGES-Pentosidine, and peak at 1655-1667 cm⁻¹ increased, stating recovery, better organization, improved structural differences and collagen quality ^{30,43,46}. A restricted collagen maturation, associated with a dose-dependent decrease of pentosidine ⁶³ was also determined, producing a worse mechanical performance of hard tissues ⁶². Samples of CAD treated with SEB·Bd-ZnCl₂ also denoted a lower sensitivity to molecular orientation to favor crystallization ⁴⁴, as α -helices (peak at 1340 cm⁻¹) decreased (Table IIb). In line with those findings, a general movement toward higher frequencies of crosslinking was observable (Table IIa), which results in improved mechanical strength and stability of dentin collagen to promote nucleation ⁴³. High crosslinking parameters and conformational changes of proteins were associated regularly with high ratios of remineralization in dentin surfaces, indicating that the first remineralization is intrafibrillar ⁷⁴.

SEB·P-ZnCl₂ and SEB·Bd-ZnO attained intermediate values of nanomechanical properties in comparison to crystals formed in specimens treated with SEB·P-ZnO and SEB·Bd-ZnCl₂ (Fig 2). After load cycling, both nanohardness (Hi) and modulus of Young (Ei) increased at the hybrid layer (Figs 2A, 2C). Raman analysis of mineral components in caries-affected dentin substrates infiltrated with SEB·Bd-ZnO and load cycled permitted to observe minerals quite similar to SEB·Bd-ZnO. This performance

lead to a relative modest signal when comparable to the emission obtained with SEB·P-ZnO and SEB·Bd-ZnCl₂, *i.e.*, higher FWHM (Table IIa).

Decreased crystallinity has been associated to increased dental caries, smaller crystal size and bigger dissolution of minerals⁷⁵. Substitution of Mg²⁺ with Ca²⁺ (Fig 7D-EDX) may have resulted in contraction of network. Declining of lattice parameter is due to the smaller atomic radius of Mg ions in comparison with Ca ions, which is approximately 0.035 nm smaller⁶⁸, comprising crystallinity. Nevertheless, SEB·P-ZnCl₂ and SEB·Bd-ZnCl₂ performed similar from Raman analysis (Table IIa), as both Zn-doped adhesives produced analogous large minerals. These new crystals of apatite observed in remineralized dentin may be due to the dissolution of carbonate and Mg-rich dentin apatite⁷⁶ and reprecipitation of carbonate and Mg-poor apatite⁷⁷. Both CO₃⁻ (carbonate) and Mg cause reduction in crystallinity of apatites (Table IIa)⁷⁸. Mg-substituted β-TCP and apatite can form simultaneously depending on the Mg/Ca in the medium from which they formed⁷⁷. Nevertheless, ZnCl₂ included into the bonding of SEB produced greater mineral deposits composed of stratified and calcified nucleus and bodies within and onto intertubular and peritubular dentin, completing a significant net remineralization (Fig 8D). On the other hand, SEB·P-ZnCl₂ applied on caries affected dentin and load cycled originated mineral formations which protruded from tubules, allowing the observation of some non-collapsed and denuded collagen fibrils (Fig 7D). This partial demineralization or exposed protein was also evidenced at the resin-dentin interface located at both intertubular and peritubular dentin areas (Fig 5F). Crosslinking and protein structures in specimens treated with both SEB·P-ZnCl₂ and SEB·Bd-ZnO performed dissimilar, presenting different phases of dentin mineralization. The low mineral content which was attained after load cycling with both doped adhesives, SEB·P-ZnCl₂ and SEB·Bd-ZnO (Figs 4 IVC, 4VIC), might have accounted for the

weaker mechanical properties that attained (Fig 2). This suggests that incorporation of Zn into the primer or bonding of SEB systems may affect the potential of dentin to be functionally remineralized. Thus, the mineral located at this zone may not be incorporated into the collagen fibrils to provide a complete recovery in mechanical properties. This result may also reflect damage of the collagen matrix which remained partially demineralized (Figs 5F, 5H), as it was demonstrated after the increase of ICTP over time, as a result of MMPs proteolytic activity⁶⁰.

It has been shown that this local increase of calcium concentration may inhibit zinc binding, depending on the relative abundance of these two divalent ions⁷⁹. The association among the *in situ* release of zinc, mineral precipitation and *in vitro* load cycling on partially demineralized and infiltrated dentin is supported by the effect of compressive loads on the stimulation of the tissue-nonspecific alkaline phosphatase⁸⁰, a zinc metalloenzyme that hydrolyzes a broad range of phosphate monoesters^{81,82}. At high phosphate concentration, calcium pyrophosphate, calcium phosphate and unstable and non-crystalline amorphous complexes are formed⁸³ around the collagen fibrils, keeping the alkaline phosphatase and other enzymes "fossilized"⁸⁴, thus hindering the complete remineralization.

Though this study represents, to the best of our knowledge the first to characterize chemical, mechanical and morphological structure of self-etching Zn-doped adhesives/caries-affected dentin interfaces, new steps on the ongoing of this research are required. To determine the influence of temperature, to incorporate new techniques as transversal microradiography (TMR) or to select some other materials as glass ionomer cements (GICs) deserve new studies in the field of caries-affected dentin therapy.

IV. CONCLUSIONS

Mechanical loading established significant differences among groups, as SEB attained greater bond strength and lower percentage of adhesive failures than the SEB-Zn doped specimens, after load cycling. In general, a substantial restoration of the mechanical properties of caries-affected dentin substrata occurred when SEB-Zn doped adhesives were used and load cycled was applied, leading to functional remineralization. ZnO incorporated into the primer of SEB system, promoted one of the highest increases in nanohardness and modulus of Young, at the resin-dentin interface, after load cycling. This finding was associated to a strong pattern of crystalline mineral deposition composed of zinc-based salts, in platforms, without any sign of demineralization. Phosphate, carbonate and the relative mineral concentration increased, though the gradient of mineral content decreased as a consequence of the bigger rise of phosphate. Resultant nucleation originated lower values of crosslinking, but improved nature of collagen, meaning recovery, better organization, structural differences and collagen quality. ZnCl₂ included into the bonding of SEB system promoted an increase of the modulus of Young at the hybrid complex, after mechanical loading. Macro and microporous crystals deposited on the dentin surface, though resin-dentin interfaces revealed some limited signs of demineralization. Both phosphates and crystallinity increased, but carbonates, the gradient of mineral content and the relative mineral concentration decreased, as a result of a lower presence of carbonates and bigger intensity of the phenyl group. Both crosslinking and nature of collagen enhanced. SEB·P-ZnCl₂ and SEB·Bd-ZnO attained intermediate values of nanomechanical properties, with decreased crystallinity, *i.e.*, smaller crystal size and bigger dissolution of minerals. Crosslinking and protein structures performed dissimilar, presenting different phases of dentin mineralization, after load cycling.

ACKNOWLEDGMENTS

This work was supported by grant MINECO/FEDERMAT2014-52036-P.

The authors have no financial affiliation or involvement with any commercial organisation with direct financial interest in the materials discussed in this manuscript.

Any other potential conflict of interest is disclosed.

REFERENCES

1. L. Bjørndal, *Oper. Dent.* **27**, 211 (2002).
2. T. Fusayama and S. Terachima, *J. Dent. Res.* **51**, 866 (1972).
3. T. Fusayama, *Oper. Dent.* **4**, 63 (1979).
4. M.K. Pugach,, J. Strother, C.L. Darling, D. Fried, S.A. Gansky, S.J. Marshall and G.W. Marshall, *J. Dent. Res.* **88**, 71 (2009).
5. D.S. Alleman and P. Magne, *Quintessence Int.* **43**, 197 (2012).
6. C. Xu and Y. Wang, *J. Biomed. Mater. Res. B Appl. Biomater.* **96**, 242 (2011).
7. B. Van Meerbeek, K. Yoshihara, Y. Yoshida, A. Mine, J. De Munck, and K.L. Van Landuyt, *Dent. Mater.* **27**, 17 (2011).
8. N. Nishiyama, M. Aida, K. Fujita, K. Suzuki, F.R. Tay, D.H. Pashley, and K. Nemoto, *Dent. Mater. J.* **26**, 382 (2007).
9. F.R. Tay and D.H. Pashley, *Dent. Mater.* **17**, 296 (2001).
10. N. Moszner, U. Salz and J. Zimmermann, *Dent. Mater.* **21**, 895 (2005).
11. K. Yoshihara, Y. Yoshida, S. Hayakawa, N. Nagaoka, M. Irie, T. Ogawa, K.L. Van Landuyt, A. Osaka, K. Suzuki, S. Minagi, and B. Van Meerbeek, *Acta Biomater.* **7**, 3187 (2011).
12. K.Yoshihara, Y. Yoshida, S. Hayakawa, N. Nagaoka, Y. Torii, A. Osaka, K. Suzuki, S. Minagi, B. Van Meerbeek, and K.L.Van Landuyt, Self-etch monomer-calcium salt deposition on dentin. *J. Dent. Res.* **90**, 602 (2011).
13. M. Peumans, J. De Munck, K.L. Van Landuyt, A. Poitevin, P. Lambrechts, and B. Van Meerbeek, *Dent. Mater.* **26**, 1176 (2010).
14. H. Nurrohman, S.Nakashima, T. Takagaki, A. Sadr, T. Nikaido, Y. Asakawa, M. Uo, S.J. Marshall, and J. Tagami, *Biomed. Mater. Eng.* **25**, 89 (2015).

15. S. Chersoni, P. Suppa, L. Breschi, M. Ferrari, F.R. Tay, D.H. Pashley, and C. Prati, *Dent. Mater.* **20**, 796 (2004).
16. N. Moszner, J. Angermann, U. Fischer, and T. Bock, *Macromol. Mater. Eng.* **298**, 454 (2013).
17. R. Osorio, M. Yamauti, E. Osorio, M.E. Ruiz-Requena, D. Pashley, F. Tay, and M. Toledano, *Eur. J. Oral Sci.* **119**, 79 (2011).
18. Y. Wang, P. Spencer, and M.P. Walker, *J. Biomed. Mater. Res. A* **81**, 279 (2007).
19. H. Ryou, L.N. Niu, L. Dai, C.R. Pucci, D.D. Arola, D.H. Pashley, and F.R. Tay, *J. Dent. Res.* **90**, 1122 (2011).
20. D.H. Pashley, F.R. Tay, L. Breschi, L. Tjäderhane, R.M. Carvalho, M. Carrilho, and A. Tezvergil-Mutluay, *Dent. Mater.* **27**, 1 (2011).
21. R. Osorio, M. Yamauti, E. Osorio, ME Ruiz-Requena, D.H. Pashley, D.H., Tay, F.R., and M. Toledano, *J. Dent.* **39**, 148 (2011).
22. A. Hoppe, N.S. Guldal and A.R. Boccaccini, *Biomaterials* **11**, 2757 (2011).
23. Y. Liu, S. Mai, N. Li, C.K. Yiu, J. Mao, D.H. Pashley, and F.R. Tay, *Acta Biomater.* **7**, 1742 (2011).
24. T. Takatsuka, K. Tanaka and Y. Iijima, *Dent. Mater.* **21**, 1170 (2005).
25. L. Zheng, J.F. Hilton, S. Habelitz, S.J. Marshall, and G.W. Marshall, *Eur. J. Oral Sci.* **111**, 243 (2003).
26. Y. Liu, X. Yao, Y.W. Liu, and Y. Wang, *Caries Res.* **48**, 320 (2014).
27. H. Koibuchi, N. Yasuda, and N. Nakabayashi, *Dent. Mater.* **17**, 122 (2001).
28. M. Toledano, M. Yamauti, M.E. Ruiz Requena, and R. Osorio, *J. Dent.* **40**, 756 (2012).

29. M. Toledano, S. Sauro, I. Cabello, T. Watson, and R. Osorio, *Dent. Mater.* **29**, e142 (2013).
30. M. Toledano, F.S. Aguilera, S. Sauro, I. Cabello, E. Osorio, and R. Osorio, *Dent. Mater.* **30**, e169 (2014).
31. S. Sauro, M. Toledano, F.S. Aguilera, F. Mannocci, D.H.Pashley, F.R. Tay, T.F. Watson, and R.Osorio, *Dent. Mater.* **27**, 563 (2011).
32. S. Sauro, R. Osorio, T.F. Watson, and M. Toledano, *J. Mater. Sci. Mater. Med.* **23**, 1521(2012).
33. M. Toledano, I. Cabello, F.S. Aguilera, E. Osorio, and R. Osorio, *J. Biomech.* **48**, 14 (2015).
34. M. Toledano, E. Osorio, F.S. Aguilera, S. Sauro, I. Cabello, and R. Osorio, *J. Mech. Behav. Biomed. Mater.* **30**, 61 (2014).
35. A. Almahdy, F.C. Downey, S. Sauro, R.J. Cook, M. Sherriff, D. Richards, T.F.Watson, A. Banerjee, and F. Festy, *Caries Res.* **46**, 432 (2012).
36. N. Nakabayashi, *Proc. Finn. Dent. Soc.* **88** (Suppl 1), 321 (1992).
37. J.W. Ager, R.K. Nalla, K.L. Breeden, and R.O. Ritchie, *J. Biomed. Opt.* **10**, 034012 (2005).
38. A.G. Schwartz, J.D. Pasteris, G.M. Genin, T.L Daulton, and S. Thomopoulos, *PLoS One* **7**, e48630 (2012).
39. K. Karan, X. Yao, C. Xu, and Y. Wang, *Dent. Mater.* **25**, 1205 (2009).
40. H. Milly, F. Festy, T.F. Watson, I. Thompson, and A. Banerjee, *J. Dent.* **42**, 158 (2014).
41. U. Daood, K. Iqbal, L.I. Nitisusanta, and A.S. Fawzy, *J. Biomed. Mater. Res. A* **101**, 1846 (2013).

42. M. Jastrzebska, R. Wrzalik, A. Kocot, J. Zalewska-Rejdak, and B. Cwalina, J. Biomater. Sci. Polym. Ed. **14**, 185 (2003).
43. C. Xu and Y. Wang, J. Adhes. Dent. **14**, 11 (2012).
44. C. Wang, Y. Wang, N.T. Huffman, C. Cui, X. Yao, S. Midura, R.J. Midura, and J.P. Gorski, J. Biol. Chem. **284**, 7100 (2009).
45. D.R. Sell and V.M. Monnier, J. Biol. Chem. **264**, 21597 (1989).
46. H. Salehi, E. Terrer, I. Panayotov, B. Levallois, B. Jacquot, H. Tassery, and F. Cuisinier, J. Biophotonics **6**, 765 (2013).
47. Y. Wang and P. Spencer, J. Dent. Res. **82**, 141 (2003).
48. V.P. Feitosa, F.A. Ogliari, B. Van Meerbeek, T.F. Watson, K. Yoshihara, A.O. Ogliari, M.A. Sinhoreti, A.B. Correr, G. Cama, and S. Sauro, J. Dent. Res. 2014; **93**, 201 (2014).
49. T. Nikaido, K.H. Kunzelmann, H. Chen, M. Ogata, N. Harada, S. Yamaguchi, C. F. Cox, R. Hickel, and J. Tagami, Dent. Mater. **18**, 269 (2014).
50. K. Koshiro, S. Inoue, T. Tanaka, K. Koase, M. Fujita, M. Hashimoto, and H. Sano, Eur. J. Oral. Sci. **112**, 368 (2004).
51. M. Toledano, R. Osorio, A. Albaladejo, F.S. Aguilera, F.R. Tay, and M. Ferrari, Oper. Dent. **31**, 25 (2006).
52. A.K. Burwell, T. Thula-Mata, L.B. Gower, S. Habelitz, M. Kurylo, S.P. Ho, Y.C. Chien, J. Cheng, N.F. Cheng, S.A. Gansky, S.J. Marshall, and G.W. Marshall, PLoS One **7**, e38852 (2012).
53. M. Balooch, S. Habelitz, J.H. Kinney, S.J. Marshall, and G.W. Marshall, J. Struct. Biol. **162**, 404 (2008).
54. Y. Li, T.T. Thula, S. Jee, S.L. Perkins, C. Aparicio, E.P. Douglas, and L.B. Gower, Biomacromolecules **13**, 49 (2012).

55. L.E. Bertassoni, S. Habelitz, J.H. Kinney, S.J. Marshall, and G.W. Marshall Jr., *Caries Res* **43**, 70 (2009).
56. B. Van Meerbeek, J. De Munck, Y. Yoshida, S. Inoue, M. Vargas, P. Vijay, K. Van Landuyt, P. Lambrechts, G. Vanherle, *Oper. Dent.* **28**, 215 (2003).
57. Y. Yoshida, K. Nagakane, R. Fukuda, Y. Nakayama, M. Okazaki, H. Shintani, S. Inoue, Y. Tagawa, K. Suzuki, J. De Munck, and B. Van Meerbeek, *J. Dent. Res.* **83**, 454 (2004).
58. B. Fu, X. Sun, W. Qian, Y. Shen, R. Chen, and M. Hannig, *Biomaterials* **26**, 5104 (2005).
59. Y. Yoshida, K. Yoshihara, N. Nagaoka, S. Hayakawa, Y. Torii, T. Ogawa, A. Osaka, and B.V. Meerbeek, *J. Dent. Res.* **91**, 376 (2012).
60. R. Osorio, M. Yamauti, E. Osorio, J.S. Román, and M. Toledano, *Eur. J. Oral Sci.* **119**, 401 (2011).
61. C. Pomacóndor-Hernández, R. Osorio, F.S. Aguilera, I. Cabello, M. de Goes, and M. Toledano, *Am. J. Dent.* 2015, In press.
62. S.Y. Tang and D. Vashishth, *Bone* **46**, 148 (2010).
63. M. Saito, S. Mori, T. Mashiba, S. Komatsubara, and K. Marumo. *Osteoporos Int.* **19**, 1343 (2008).
64. I.V. Fadeev, L.I. Shvorneva, S.M. Barinov, and V.P. Orlovskii, *Inorg. Mater.* **39**, 947 (2003).
65. F.C.M. Driessens and R.M.H. Verbeeck, *Bull. Soc. Chim. Belg.* **91**, 573 (1982).
66. R.Z. LeGeros, *J. Dent. Res.* **69** Spec No, 567 discussion 634 (1990).
67. G. Daculsi, R.Z. LeGeros, and A. Jean, *J. Dent. Res.* **66**, 1356 (1987).
68. S. Hesarakı, S. Farhangdoust S, K. Ahmadi, R. Nemati, and M. Khorami, *J. Aust. Ceram. Soc.* **2**, 166 (2012).

69. F.C. Driessens, J.W. van Dijk, and J.M. Borggreven, *Calcif. Tissue Res.* **26**, 127 (1978).
70. L. Tjäderhane, E.L. Hietala, and M. Larmas, *J. Dent. Res* **74**, 1770 (1995).
71. L.E. Bertassoni, S. Habelitz, and M. Pugach, *Scanning* **32**, 312 (2010).
72. M. Toledano, R. Osorio, A. Albaladejo, F.S. Aguilera, and E. Osorio, *J. Biomed. Mater. Res. A* **77**, 128 (2006).
73. Brown ID, *The chemical bond in inorganic chemistry: the bond valence model* (Oxford University Press, Oxford, 2006).
74. M. Toledano, F.S. Aguilera, I. Cabello, and R. Osorio, *Biomech. Model. Mechanobiol.* **13**, 1289 (2014).
75. B.T. Amaechi, N. Porteous, K. Ramalingam, P.K. Mensinkai, R.A. Ccahuana Vasquez, A. Sadeghpour, and T. Nakamoto, *Caries Res.* **47**, 399 (2013).
76. R.Z. LeGeros, *Prog. Cryst. Growth Charact.* **4**, 1(1981).
77. R.Z. LeGeros and M.S. Tung, *Caries Res.* **17**, 419 (1983).
78. R.Z. LeGeros, R. Kijkowska, and J.P. LeGeros, *Scan. Electron Microsc.* **Pt 4**, 1771(1984).
79. K. Rosenberg, H. Olsson, M. Mörgelin, and D. Heinegård. *J. Biol. Chem.* **273**, 20397 (1998).
80. T.N. McAllister and J.A. Frangos, *J. Bone Miner. Res.* **14**, 930 (1999).
81. P.A. Price, D. Toroian and W.S. Chan, *J. Biol. Chem.* **284**, 4594 (2009).
82. A.S. Posner, N.C. Blumenthal, and A.L. Boskey, *Kidney Int. Suppl.* **18**, S17 (1986).
83. P.T. Cheng and K.P. Pritzker, *J. Rheumatol.* **10**, 769 (1983).
84. B. Van Meerbeek, S. Vargas, S. Inoue, Y. Yoshida, M. Peumans, and P. Lambrechts, G. VanHerle, *Oper. Dent.* **26**, S119 (2001).

FIGURE CAPTIONS

Fig 1. Microtensile bond strength values (MPa) and percentage distribution of failure mode obtained for the different experimental groups. Asterisks indicate significant difference after Student-Newman-Keuls or Student's t tests ($p < 0.05$). No differences were found between load and unloaded groups. Abbreviations: A: Adhesive failure; M: Mixed failure; SEB: SE-Bond; SEB·P: SE-Bond primer; SEB·Bd: SE-Bond bonding; ZnO: zinc oxide; ZnCl₂: zinc chloride.

Fig 2. Mean and SD of Nanohardness (GPa) (A, B) and Young Modulus (GPa) (C, D) measured at the experimental hybrid layers (HL) and bottom of hybrid layer (BHL) in caries-affected dentin (CAD) specimens. Identical letters indicate no significant differences between unloaded restorations within the different experimental adhesives. Identical numbers indicate no significant differences between load cycled restorations within the different experimental adhesives and * indicate significant differences between unloaded and load cycled restorations within the same experimental adhesive. Abbreviations: SEB, SE-Bond. SEB·P, SE-Bond primer. SEB·Bd: SE-Bond bonding. ZnO, zinc oxide. ZnCl₂, zinc chloride.

Fig 3. Bi-dimensional (2D) micro-Raman map of the phosphate peak (961 cm^{-1}) intensities (A) and K-means clustering (KMC) map of the Raman profile of the same sample (B), at the dentin-bonded interface of SEB-treated caries-affected dentin surfaces, unloaded (I), or load cycled (II). The color of the scale corresponds to the intensity of the Raman scattered light; red represents high intensity of phosphate peak and dark blue represents low intensity of phosphate peak. The plot is oriented such that the adhesive is in the lower aspect of the image and the dentin is in the upper aspect.

Raman *spectra* of principal components (PCs) is also observed (C): ADH, adhesive; HY COM, hybrid complex; DEN1 and DEN2, dentin.

Fig 4. Bi-dimensional (2D) micro-Raman map of the phosphate peak (961 cm^{-1}) intensities (A) and K-means clustering (KMC) map of the Raman profile of the same sample (B), at the dentin-bonded interface of SEB·P-ZnO doped unloaded (I) or load cycled (II), SEB·P-ZnCl₂ doped unloaded (III) or load cycled (IV), SEB·Bd-ZnO doped unloaded (V) or load cycled (VI), and SEB·Bd-ZnCl₂ unloaded (VII) or load cycled (VIII). The color of the scale corresponds to the intensity of the Raman scattered light; red represents high intensity of phosphate peak and dark blue represents low intensity of phosphate peak. The plot is oriented such that the adhesive is in the lower aspect of the image and the dentin is in the upper aspect. Raman *spectra* of principal components (PCs) are also observed (C): ADH, adhesive; HY COM, hybrid complex; DEN1 and DEN2, dentin.

Fig 5. Representative light micrographs of SEB adhesive systems in caries-affected dentin (CAD) specimens; interfaces stained with Masson's trichrome: mineralized dentin stained green, adhesive stained beige, and exposed protein stained red. Original magnification: 150X. (A): SEB control (unloaded). (B): SEB load cycled. (C): SEB·P-ZnO unloaded. (D): SEB·P-ZnO load cycled. (E): SEB·P-ZnCl₂ unloaded. (F): SEB·P-ZnCl₂ load cycled. (G): SEB·Bd-ZnO unloaded. (H): SEB·Bd-ZnO load cycled. (I): SEB·Bd-ZnCl₂ unloaded. (J): SEB·Bd-ZnCl₂ load cycled. Limited and clear resin uncovered decalcified dentin is shown (asterisk) (A). Evidence of partial demineralization or exposed protein may be detectable at the resin-dentin interface located at both intertubular (asterisks) and peritubular (arrows) dentin areas (B, C, E, F,

G, H). Slight and faint signs of demineralization show the scarce exposed proteins detected (pointers) (G, I, J). No signs of demineralization or exposed protein (red stain), *i.e.*, absence of unprotected collagen layer is detectable at the resin/dentin interface; clear observation of histological remineralization of the partially demineralized dentin layer is detected (double arrows) (D). Abbreviations: SEB, SE-Bond. SEB·P, SE-Bond primer. SEB·Bd: SE-Bond bonding. ZnO, zinc oxide. ZnCl₂, zinc chloride.

Fig 6 Field-emission scanning electron microscopy images of failures after bonding and microtensile bond strength testing. (A) SEB unloaded. (B) SEB load cycled. Mixed failures and fracture at the bottom of hybrid complex may be observed in SEB unloaded specimens (A). Collagen fibers are clearly observed at intertubular dentin, some of them partially mineralized (asterisk), or resin-infiltrated (double arrow), permitting to observe the presence of mineral crystals embedded in a remnant resin/collagen scaffold-like structure. Some non-sealed (arrow) tubules turned up mineral filled or appeared totally empty (pointer), allowing to observe the non-dissolved peritubular dentin. SEB load cycled sample (B) showed a mixed failure with the main fracture at the top of the hybridized complex. Intertubular dentin permits to observe a dense network of scales-shaped mineralized fibrils (asterisk). The mineral is covering partially (arrow) or totally (double arrow) the entrance of tubules. The prototypical D-periodicity banding of peritubular coating collagen fibrils was observed in multiple details (pointer), at high magnifications.

Fig 7. Field-emission scanning electron microscopy images of failures after bonding and microtensile bond strength testing (A) SEB·P-ZnO unloaded. (B) SEB·P-ZnO load cycled. (C) SEB·P-ZnCl₂ unloaded. (D) SEB·P-ZnCl₂ load cycled. SEB·P-ZnO

unloaded (A) showed a mixed failure at the bottom of the hybrid complex. Multiple clumps of precipitated minerals appeared covering both intertubular and peritubular dentin (asterisks), but allowing the visual observation of tubule walls. Zinc-based salts [phosphorous (P), calcium (Ca), and zinc (Zn)] were detected in the elemental analysis (EDX, spectrum 38). When SEB·P-ZnO load cycled (B) was analyzed, a mixed failure of the hybrid complex was observable. Net-shaped precipitated crystals appeared covering the intertubular and peritubular dentin. A first layer of crystal nucleation may be detected throughout the net (pointer). Crystals nucleated coating the collagen fibrils and permitting the observation of the periodicity banding (arrow). SEB·P-ZnCl₂ unloaded (C) showed a mixed failure at the bottom of the hybrid complex. A consistent and continuous layer of mineral is observed covering the intertubular dentin (asterisk). Mineralized collagen fibrils are noticeable below this coat of new crystals (arrow). The typical staggered pattern of those collagen fibrils, due to the characteristic D-periodicity (67 nm), is visible. Isolated mineral precipitates linked by mineralized fibers (pointer) or occupying the lumen of tubules are also observable (double arrow). Spectrum from energy dispersive analysis, attained at zone 43 is showing elemental composition of phosphorous (P), calcium (Ca) and zinc (Zn). SEB·P-ZnCl₂ load cycled (D) showed a mixed failure at the top of the hybridized complex. Failure surface analysis permitted to observe a thicker and extended platform of mineral, at intertubular dentin. These crystal formations did not allow to see the subjacent collagen fibers. Some terminal knob-like mineral structures are exhibited on the interface (arrows). Tubules appeared mineral-occupied without hermetic sealing (pointer). Spectrum from energy dispersive analysis, attained at zone 46, is showing elemental composition of phosphorous (P), calcium (Ca), magnesium (Mg) and zinc (Zn).

Fig 8. Field-emission scanning electron microscopy images of failures after bonding and microtensile bond strength testing. (A) SEB·Bd-ZnO unloaded. (B) SEB·Bd-ZnO load cycled. (C) SEB·Bd-ZnCl₂ unloaded. (D) SEB·Bd-ZnCl₂ load cycled. SEB·Bd-ZnO unloaded (A) produced a mixed failure at the bottom of the hybrid complex. Crystals precipitated in bigger and inter-connected knob-like formations. Collagen fibrils appeared longitudinally mineralized, rounding the entrance of tubules (arrows). Any collar of peritubular dentin was observable. Tubules were mineral-filled, forming detachment gaps (pointer). Espectrum from energy dispersive analysis, attained at zone 41, is showing elemental composition of phosphorous (P), calcium (Ca), and zinc (Zn). After using SEB·Bd-ZnO load cycled (B), a mixed failure at the bottom (b) and top (t) of the hybrid complex was present. Mineral precipitates throughout the dense network of multilayered crystals on the dentin surface were shown (arrows). Clear rings of peritubular dentin were visible (pointer). Tubules appeared hermetically (double arrow) or partially (asterisk) sealed, or mineral free with a robust peritubular dentin wall (pointer). SEB·Bd-ZnCl₂ unloaded specimens (C) originated a mixed failure at the hybrid complex, both cohesive (c) and adhesive (a). Extensive labyrinth of crystal anastomoses below a remnant resin layer (a) were perceptible. This net like-mineral macro and microporous deposition is completely covering the dentin surface. Fibers appeared longitudinally mineralized, and the typical staggered pattern of collagen was visible at bigger magnifications (arrow). Espectrum from energy dispersive analysis, attained at zone 65, is showing elemental composition of phosphorous (P), calcium (Ca), magnesium (Mg) and zinc (Zn). (D) SEB·Bd-ZnCl₂ load cycled specimens showed a mixed failure at the top of the hybridized complex. Dentin (intertubular and peritubular) was strongly mineralized. The bulk of mineral formations only allowed a restricted display of the tubule entrances (asterisks), with precipitated in progressive

strata until the complete sealing of the lumen of tubule (arrow). The characteristic D-periodicity (67 nm) was revealed (pointer). Espectrum from energy dispersive analysis, attained at zone 62, is showing elemental composition of phosphorous (P), calcium (Ca), and zinc (Zn).